UNIVERSITY OF WINNIPEG

MASTER THESIS

Mathematical Modelling and Validation of Mitogenic Signaling Pathway in Breast Cancer

Author:
Abinash MEHER

Supervisor:
Dr. Anuraag SHRIVASTAV

A thesis submitted in fulfillment of the requirements for the degree of Master of Science

in the

University of Winnipeg
Department of Biological Science, Technology and Public Policy

February 25, 2022

Declaration of Authorship

I, Abinash MEHER, declare that this thesis titled, "Mathematical Modelling and Validation of Mitogenic Signaling Pathway in Breast Cancer" and the work presented in it are my own. I confirm that:

- This work was done wholly or mainly while in candidature for a research degree at this University.
- Where any part of this thesis has previously been submitted for a degree or any other qualification at this University or any other institution, this has been clearly stated.
- Where I have consulted the published work of others, this is always clearly attributed.
- Where I have quoted from the work of others, the source is always given. With the exception of such quotations, this thesis is entirely my own work.
- I have acknowledged all main sources of help.
- Where the thesis is based on work done by myself jointly with others, I have made clear exactly what was done by others and what I have contributed myself.

Signed:

Date:

Abstract

Applied Mathematics is becoming an integral part of predicting disease progression, including cancers. Mathematical models can be used to test novel hypotheses, develop optimized treatments schema and personalised therapies, and predict the outcomes. Remarkable advancements have been made in treating cancers, especially breast cancers. The phenomenal progress in computational capacities has helped make whole-genome sequencing rapid and affordable, enabling precision cancer therapy. There are many molecular drivers of breast cancer. Some of them define the breast cancer sub-types. The presence of estrogen receptor (ER, progesterone receptor (PR) and/or human epidermal growth factor 2 (HER2) or their absence defines the breast cancer subtypes and their treatment regimen. About 70% of the breast cancer diagnosed are ER/PR positive and are also known as hormone receptor-positive (HR+) breast cancer. The prognosis and treatment response of HR+ breast cancer is good for patients undergoing endocrine therapy. Despite the better prognosis of HR+ breast cancer, the recurrence rate and resistance to endocrine therapy is observed in many HR+ breast cancer cases.

The resistance to endocrine therapy and recurrence is partly attributed to the activation of the insulin pathway and independent of HR+ breast cancer cells on ER pathway for their growth. Earlier, the crosstalk between insulin and ER pathways was demonstrated. N-myristoyltransferase (NMT) exists in human in two isoforms (NMT1 and NMT2) that catalyzes myristoylation reaction. Recent research from out laboratory has shown that NMTs are vital players in the pathogenesis of JR+ breast cancer. Furthermore, it was also demonstrated from previous studies from our laboratory that NMTs are

downstream targets of insulin and ER pathways. In this thesis, I have designed mathematical models using differential equations to study the activation of the insulin pathway and its effect on NMT. The mathematical modeling incorporated the partition of cellular organelles and the sequential flow of information with cascades of equations representing signaling reactions. The activated mathematical model was designed by activating the insulin receptor (IR) or insulin-like growth factor receptors (IGF1R) and compared with the control model. The mathematical models were validated by wet-lab experiments. The HR+ breast cancer cells, MCF7 cells, were treated with insulin of IGF1 for the short-term and long-term. The status of the pathway proteins in terms of expression, localization and activity were determined by cell fractionation and Western analysis. The results revealed the correlation between the differential expression patterns of NMT and the proliferation of MCF7 cells when the insulin pathway was activated by insulin or IGF. The mathematical modeling was validated by simulations and data fittings. The results demonstrated that differential equation based mathematical modeling could predict the NMT related oncogenic changes in ER+ breast cancer cells.

Acknowledgements

I have received a great deal of support and assistance throughout the writing of this thesis and making it to completion. I would like to express my sincere thanks to all of them who have been a part of it directly or indirectly and would like to mention a few of them here:

Foremost, I would like to express my deepest appreciation to my parents and my sisters who were there at every step of my life as pillars. Their constant love and faith in me have uplifted me when I needed them the most. Being an international student, imposter syndrome is something very hard to avoid and it is their love which gave me strength to fight.

I am deeply indebted to my supervisor, **Dr. Anuraag Shrivastav** for taking me as his graduate student. Having a mathematics background and no knowledge of the new biology work environment was very scary for me. Especially, when I had no idea where to even begin. His faith in me and his constant push led me to work harder. It is a field where rate of getting success is very low compared to failures in experiments since there are thousands of things that could go wrong. Frustration is inevitable and this is where his way of learning not only in a classroom or lab, but also from life itself helped me to dig deeper and reach higher. During the pandemic when it was desperate time and whole planet was under lockdown, he presented himself not only as a mentor but also as a family to me for which I will forever be in debt. Thank you so much Dr. Shrivastav.

I am extremely grateful to my committee members **Dr. Stephanie Portet** and **Dr. Sara Good** for sharing their precious time and giving me advice on my thesis work and for the discussions which helped me see the bigger picture which I was lacking. I also would like to extend my appreciation

to **Dr. Shaily Verma Shrivastav** not only for her support but also for her creative ideas towards the analysis of my results.

I would like to extend my gratitude to **Dr. Palok Aich**, NISER. After I graduated from NISER, the project I did under him, became my stepping-stone and guided me towards this direction and changed my life. Thank you Dr. Aich.

Many many thanks to my lab-mates **Dean Reddick**, **Apurva Bhardwaj**, **Shiby Kuriakose**, **Revanti Mukharjee**, **Anouska Agarwal**, and my friend **Simran Sandhu** for being there to teach me and assist me with the lab work and for brainstorming sessions. It takes one to know one. In this case, a grad student knows perfectly what the other student is going through and when to take a break. Thank you for all the trips we had to Tim Hortons, for all the fun we had in the lab and outside the lab, for standing there with me through thick and thin.

Last but not least, I would like to thank myself for putting myself up without giving up everytime I had an unsuccessful experiment, because no one else can walk down the road for you.

Contents

List of Figures

List of Tables

List of Abbreviations

Akt	Protein kinase β
BCA	Bicinchoninc Acid
BSA	Bovine Serum Albumin
c-Src	Cellular sarcoma proto oncogene tyrosine protein
DMEM	Dulbecco's Modified Eagle Media
DNA	Deoxyribonucleic acid
EDTA	Ethylenediaminetetraacetic acid
EGFR	Epidermal growth factor receptor
ER	Estrogen receptor
ER+	Breast cancer cells expressing estrogen receptor
ERα	Estrogen receptor alpha
ERβ	Estrogen receptor beta
FBS	Feta bovine serum
GFP	Green fluorescent protein
IGF	Insulin like growth factor
IGF1	Insulin like growth factor 1
IGF2	Insulin like growth factor 2
IGF1R	Insulin like growth factor receptor
IRS	Insulin receptor substrate
MCF7	Michigan Cancer Foundation 7 (Human ER+ Breast Cancer Cells)
mRNA	Messenger ribonucleic acid
mTOR	Mammalian target of rapamycin
NMT1	N-myristoyltransferase 1

NMT2	N-myristoyltransferase 2
p-IGF1R	Phosphorylated insulin like growth factor receptor
p-mTOR	Phosphorylated mammalian target of rapamycin
p-NMT2	Phosphorylated N-myristoyltransferase 2
P-Site	Phosphorylation site
PBS	Phosphate buffer saline
PBST	Phosphate buffer saline with tween 20 detergent
PCR	Polymerase chain reaction
PDK1	Phosphoinositide dependent kinase 1
PIP-2	Phosphatidylinositol 4,5-biphosphate
PIP-3	Phosphatidylinositol 3,4,5-triphosphate
PI3K	Phosphoinositide 3-kinase
PTEN	Phosphate and tensin homologue
PVDF	Polyvinylidene difluoride
RNA	Ribonucleic acid
RTK	Receptor tyrosine kinase
SDS PAGE	Sodium dodecyl sulphate polyacrylamide gel electrophoresis
DDE	Delayed Differential Equation
ODE	Ordinary Differential Equation

List of Variables

Symbol	State Variable
I_1	IGF1R protein
I_{1p}	Phosphorylated IGF1R
I_{1r}	IGF1R (mRNA)
T	mTOR
T_p	Phosphorylated mTOR
N	NMT2 protein
N_p	Phosphorylated NMT2
N_p^n	Phosphorylated NMT2 in the nucleus of cell

Symbol	Parameters
α_X	Catalysis constant for X
Π	Baseline production constant
π	Synthesis factor
δ_Y	Degradation constant for Y
δ	DNA binding factor
V_n	Volume of nucleus of a cell
V_c	Volume of the cytoplasm of the cell
K_Z	Michelis-Menten Constant for the state variable Z
μ	Scalar factor

List of Reagents Used

Reagents	Details
DMEM powder	gibco, Cat# 31600034
FBS (500ml)	CORNING Cellgro, Product# 35-077-CV
Penicillin Streptomycin Solution	Global Cell Solution (100ml), Cat# GSP-0800-106
L-glutamine (100ml)	CORNING Cellgro, Ref# 25-005-CI
L-glutamine (100ml)	Global Cell Solution, Cat# GSP 0500106
L-glutamine (100ml)	VWR, Product# 02-0131-0100
D-Glucose (500g)	amresco, Lot# 3573C304
0.25% Trypsin-EDTA (1X)	gibco, Product# 25200-072
Sodium Chloride (12kg)	Anachemia, Product# 81708-620
Potassium Chloride (1kg)	EMD Chemicals, Product# 7447-40-7
Sodium Pyrophosphate Dibasic (500g)	Sigma, Product# 7758-16-9
Sodium Pyrophosphate Anhydrous (2.5kg)	EMD Chemicals, Product# 7722-88-5
Potassium Phosphate, Monobasic	VWR, Product# 10049-21-5
Sodium Bicarbonate (500g)	Sigma, Product# 144-55-8
Nuclear and Cytoplasmic Extraction Kit	Thermo scientific, Cat# PI78833
Cytoplasmic Extraction Reagent I	Thermo scientific, Ref# 78833A
Cytoplasmic Extraction Reagent II	Thermo scientific, Ref# 78833B
Nuclear Extraction Reagent	Thermo scientific, Product# 78833C
Trypan Blue Stain 0.4%	GibcoBRL Life Technologies, Cat# 15250-061
Insulin, Human Recombinant	Sigma, Cat# 91077C
BCA protein assay Reagent Kit	Thermo scientfic, Cat# PI23225
BCA protein assay Reagent A	Thermo scientfic, Ref# 23228

BCA protein assay Reagent B	Thermo scientfic, Product# 1859078
Ultra pure Distilled Water	Invitrogen, Ref# 10977-015
Acrylamide (1kg)	Sigma, Product# A8887
Sodium Dodecyl Sulphate (1kg)	Amresco, Product# 151-21-3
TRIS (5kg)	VWR life science, Product# 0497
Glycine (5kg)	Fisher Bioreagents, Product# BP381-5
N,N,N,N-Tetramethylethylenediamine	Sigma life science, Product# T9281
Dimethyl sulphoxide (1L)	Sigma life science, Product# D4540-1L
β-mercaptoethanol	gibco, Ref# 21985-023
Lysis Buffer	BD Biosciences, Cat# 555899
Methanol	EMD Chemicals, Product# MX0485-3
Western ECL Substrate	Bio-Rad, Product # 1705061
Anti-NMT2 pAb (Rabbit)	Sigma Prestige, Product# HPA001303
Anti-IGF1R pAb (Rabbit)	Sigma, Product# SAB2101136
mTOR(7C10) mAb (Rabbit)	Cell Signalling Technology, Product# 2983S
p-mTOR(S2448) mAb (Rabbit)	Cell Signalling Technology, Product# 2971S
p-AKT(T308) mAb (Rabbit)	Cell Signalling Technology, Product# 2965S
Anti β-actin mAb (Mouse)	Sigma life science, Product# A5441-2ml
Anti-Lamin mAb (Mouse)	Sigma life science, Product# SAB4200236
Anti- α-tubulin mAb (Mouse)	Sigma life science, Product# T9026-100ul
E.Z.N.A Total mRNA Kit I	Omega bio-tek, R6834-02
TRK Lysis Buffer	Omega Bio-tek, Lot# TRK042115JC1417
RNA Wash Buffer I	Omega Bio-tek, Lot# RW1A062315JC1537
RNA Wash Buffer II	Omega Bio-tek, Lot# RW2A030215JC1281
DEPC Water	Omega Bio-tek, Lot# A031513QG05

Dedicated to my Parents...

Chapter 1

Introduction

+

While mathematical modelling and computational science are becoming an integrated part of every research, some molecular and cell biologist often question the requirement of mathematical modelling to understand the dynamics of biological processes. The complexity of the biological systems is yet to be understood in many ways. Mathematical modelling provides a higher level of extrapolation required to uncoil the mysteries and provide insights into the complex systems. Experimentation, observation, prediction are the pivots of research, and computational tools integrate this plethora of experimental observations and predictions. The prediction reliability depends on factors such as the availability of quantitative data on the subjects for the calibrating mathematical models.

1.1 Motivation

Cancer is a broad term for the diseases associated with the onset of uncontrolled growth and cellular division. It begins in the cells, which are the basic building blocks that make up tissue, and our body. A typical cell grows and divides to form new cells according to the body's needs and when they are old or damaged new cells take their place. But in case of cancer, this orderly process breaks down. The abnormal cells instead of dying, keep dividing and

forming new cells even when they are not needed. These extra cells form tumors. Cancerous tumors could be malignant and have an increased rate of cell division compared to normal cells, and they avoid signals of apoptosis, which can evade the body's immune system [53]. There are different types of cancer including carcinomas, sarcomas, lymphomas, leukemia, etc, known to affect human cells [55]. Cancer metastasizes to other parts of the body starting from its primary site. Cancer is named for the place it began regardless of where it spreads. For example, breast cancer that spreads to the liver is called metastatic breast cancer, not liver cancer.

Breast cancer is the most diagnosed form of cancer among women worldwide [59]. It could occur both in men and women, but it's far more common in women. It was one of the most diagnosed cancers among women in Canada over the age of 20 in 2019 and is regarded as the most lethal cancer [60]. Breast cancer may not cause any symptoms in the early stages, and the tumor may be tiny to be felt. Signs and symptoms of the most common breast cancer may include pain in the breast, swelling in some parts of the breast, swelling in some parts of the breast, redness of the skin texture over the breast, breast lump; inverted nipple; change in size or shape of the breast.

1.2 Breast Cancer Facts

In the United States

- it was estimated to have 281,550 new cases of invasive breast cancer diagnosed in women in 2021 as well as 49,290 new cases of non-invasive breast cancer cases [54];
- An estimated 43,600 women will die from breast cancer in 2022;
- 1 in 8 women will be diagnosed with breast cancer in her lifetime;
- There are over 3.5 million breast cancer survivors;

- On average, every 2 minutes a woman is diagnosed with breast cancer.

In Canada

- breast cancer is one of the most common kind of cancers in Canadian women with the exception of non-melanoma skin cancer [61, 2];
- It was estimated that in 2019, 26,900 Canadian women were diagnosed with breast cancer and 27,400 in 2020, which represents 25% of all new cancer cases in women.
- 5100 women died from it which is 13% of all cancer deaths in women.
- 1 in 8 women is expected to develop breast cancer in her lifetime and 1 in 33 will die of it according to the estimation.
- On average, 75 women will be diagnosed with breast cancer everyday and 14 will die from it every day.

1.3 Types of Breast Cancer

Breast cancer can develop in different areas of the breast, such as in the ducts and lobules. Breast cancer is categorized into the following types based on the site of origin, metastatic potential and invasiveness:

- Ductal Carcinoma In Situ (DCIS)
- Invasive Ductal Carcinoma (IDC)
- Lobular Carcinoma In Situ (LCIS)
- Invasive Lobular Carcinoma (LCS)
- Inflammatory Breast Cancer
- Metastatic Breast Cancer

Furthermore, there are five molecular subtypes of breast cancer based on the genes a cancer expresses:

- **Luminal A** is hormone receptor positive (estrogen receptor and/or progesterone receptor positive), Human Epidermal Growth Factor Receptor 2 (HER2) negative, and has low level expression of the protein Ki-67, which is a cellular proliferation indicator [15].

- **Luminal B** breast cancer is hormone receptor positive, either HER2 positive or negative with high levels of Ki-67. The growth rate of Luminal B breast cancer is faster than Luminal A type breast cancer and their prognosis could be slightly worse.

- **Triple Negative** breast cancer is hormone receptor negative and HER2 negative which means the growth of cancer in this type is not fueled by hormones or by the HER2 mediated pathway. Hence, it doesn't respond to hormonal therapy or HER2 targeted therapy.

- **HER2 enriched** breast cancer is hormone receptor negative but overexpresses HER2 protein. This type of cancer tends to grow faster than luminal type cancers but often successfully treated with targeted therapies aimed at the HER2 protein.

- **Normal like** breast cancer is similar to Luminal A type breast cancer. It is hormone receptor positive, HER2 negative and has low level expression of Ki-67 although it shows a slightly worse prognosis compared to Luminal A breast cancer [1].

1.4 Diagnosis and Treatment

Breast cancer is the most prevalent cancer among women worldwide. Due to the recent advances in screening methods and breakthroughs, the survival

rate has increased dramatically. Notably, advancements in molecular biology have aided in a better understanding of the oncogenic-signaling pathways.

Breast cancer is diagnosed though multiple tests such as mammogram, ultrasound, MRI, etc.

- A **Mammogram** is an X-ray of the breast [23]. In this world of technology, the advantages of a digital mammogram includes the use of computer aided detection and algorithm-based computer programs that can alert to possible abnormalities. It is used to detect abnormalities, after some signs of breast cancer such as a lump in the breast, thickening of the skin on the breast. [54].

- **MRI** or Magnetic Resonance Imaging transmits harmless radio waves through the breast tissue to scan it and produces high-resolution images. The high sensitivity of MRI enables the early diagnosis of breast cancer. It's high sensitivity in the detection of Invasive Ductal Carcinoma has been reported [28].

- **Breast Biopsy** is the removal of a small amount of tissue or fluid from a suspicious area for examination under a microscope. It is the only method that could definitely determine the presence or absence of cancer in the suspicious area. The different types of breast biopsies include fine needle aspiration biopsy, core needle biopsy and surgical biopsy [57].

1.4.1 Treatment

Conventional methods of treatment of breast cancer involve surgery, radiation therapy, chemotherapy, endocrine (hormone) therapy and targeted therapy [58].

- **Surgery** is the trending approach in localized breast cancer treatment where tumor is removed, including some surrounding healthy tissues, followed by adjuvant therapy to minimize any risk of metastases [12]. Lumpectomy and Mastectomy are the two common types of surgery.

- **Adjuvant therapy** is given based on the individual risk of relapsing and predicted sensitivity to any particular treatment. It should be based on the surrogate intrinsic phenotype determined by the assessment of estrogen receptor(ER) or progesterone receptor(PR), HER-2, and Ki-67 according to 2013 *St. Gallen* guidelines [4][58].

- There are many types of **chemotherapy** used to treat breast cancer, where the common drugs include *docetaxel* and *doxorubicin*. They target cancer cells by thwarting them from growing and dividing. It is mostly used in ER negative tumors.

- **Endocrine therapy** is an effective treatment for tumors that test positive for estrogen and/or progesterone receptors which fuels the growth of tumor cells. Blocking hormones helps prevent the recurrence of cancer. It is also used after chemotherapy [39]. The medication choice depends on the menopausal status of the patients and their side effects profile [39].

- **Targeted therapy** is a treatment where it targets specific genes, and proteins responsible for cancer growth. For example, *Trastuzumab* is used combined with chemotherapy in patients with overexpression of HER-2 to reduce the recurrence risk [38].

1.5 ER positive Breast Cancer

Estrogen receptor positive or ER+ breast cancer is the most common type of breast cancer diagnosed, and accounts for 75% of all diagnosed breast cancer

cases, of which 65% are also progesterone receptor (PR) positive [8, 52]. Thus, it is followed by surgery in the majority of patients. Estrogen receptors (ERs) are nuclear proteins that regulate specific genes. Hormone receptor positive breast cancer cells overexpress ER or PR and fuels the growth of cancer cells by activating the hormone dependent signaling pathways regulating cell proliferation.

ER exists in two isoforms, ERα and ERβ encoded by genes present in chromosome 6 and 14, respectively. They also can homo-dimerize or hetero-dimerize for their transcription action mediation. Each ER subtypes displays a unique role in gene regulation and alters different signaling pathways downstream [11]. ERα is found to be overexpressed in ER+ breast cancer cells, due to which it is used as a primary biomarker for the diagnosis of ER+ breast cancer [29]. The substantial influence of ER on breast cancer leads to the logical assumption that ER and it's downstream targets might be the leading cause of resistance to endocrine therapy.

1.6 Selective Estrogen Receptor Modulators (SERM)

ERα is overexpressed in over half of the breast cancers, and approximately 70% of those respond to anti-estrogen therapy [44]. But about 50% of all patients with primary breast cancer tumors develop resistance to tamoxifen, an ER antagonist in mammary tissue, by competitively inhibiting endogenous estrogen molecules from binding to the ER active sites [17][30]. The development of resistance is still unclear and yet to be understood.

1.7 N-myristoyltransferase (NMT)

Myristoylation is a process of irreversible lipid modification where a 14 carbon saturated fatty acid is covalently attached onto an N-terminal glycine

residue of a polypeptide [42]. This modification can be added either co-translationally or post-translationally and can be found to occur in animals, plants, fungi and viruses [48, 49, 32, 26]. This reaction is catalyzed by an enzyme N-myristoyltransferase (NMT). Myristoylation is a crucial process that allows target proteins to become active and functional, including physiological activities such as cell signaling, signal transduction, and cellular transformation.

1.8 NMT and Cancer

NMT has been found to exist in two forms, NMT1 and NMT2, in mammals and higher vertebrates and share 77% amino acid homology. The structural changes resulting from the modifications due to NMT affect on cellular localization and protein activity [47, 46]. In humans, they have shown to be up-regulated in several types of diseases including colorectal cancer, gallbladder cancer, and brain tumors, and hence are potential therapeutic targets in cancer [16, 40, 42, 5].

1.9 Mitogenic Breast Cancer Signaling Pathway

The mitogenic signaling pathway in figure 1.1 is involved in cell growth, cell division, cell survival, migration, and transformation. It is also found to be dysregulated in many types of cancers, such as lung cancer, ovarian cancer including ER+ breast cancer, as a result of crosstalk between ER and proteins involved in the pathway [10]. This pathway is triggered by insulin, and growth factors such as EGF and IGF1, which bind to the insulin receptors, a homodimeric receptor tyrosine kinase (RTK). When bound, insulin growth factor 1 receptor (IGF1R) transmembrane proteins undergo a conformational change followed by receptor dimerization and auto-phosphorylation within

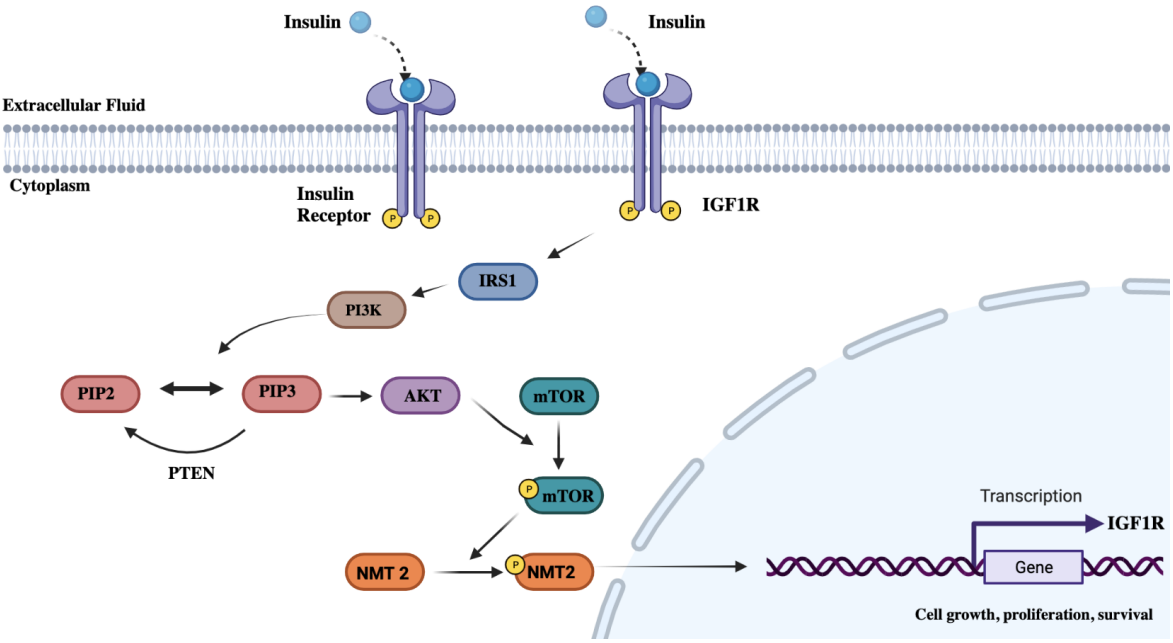

FIGURE 1.1: This is a simplification of the mitogenic signaling pathway in breast cancer having the interaction with mTOR and NMT2.

the dimer. The receptor then activates cytoplasmic insulin receptor substrate (IRS) docking protein by recruiting and phosphorylating several tyrosine residues on it. Following this, IRS binds and activates downstream PI3K, which leads to catalyzing the phosphorylation of phosphatidylinositol-4,5 diphosphate (PIP2) to phosphatidylinositol-3,4,5 triphosphate (PIP3) on the inner surface of the plasma membrane [20]. The reverse reaction of PIP3 to PIP2 is catalyzed by tensin homolog (PTEN) [51]. The PIP3 protein binds to the Pleckstrin homology (PH) domain of Akt, a serine/threonine protein kinase, and this binding exposes threonine 308 (T308) and serine 473 (S473) residues of Akt. In ER+ breast cancer cells, Akt becomes active by phosphorylating T308 and S473, which activates mTOR complex 1 (mTORC1) by phosphorylating it. mTORC1 is a kinase that regulates cell growth and proliferation [20] [41]. Preliminary studies in *Dr. Shrivastav's* lab have demonstrated the possible interaction between mTOR and NMT1 and potentially

phosphorylation of NMT1 which influences its localization patterns. The cytoplasmic and nuclear localization patterns of NMT1 and NMT2 are vital to understanding ER+ breast cancer pathogenesis and progression. The initial studies from *Dr. Shrivastav's* lab indicate the potential role of NMTs in gene transcription and cellular proliferation. Mathematical modeling of NMT regulated pathway and breast cancer progression may help better understand the HR+ breast cancer and design appropriate treatment regimens.

Chapter 2

Study Rationale, Hypotheses and Objectives

2.1 Study Rationale

Mathematics has been an integral part of biology from as early as the 13th century when the great Mathematician *Fibonacci* used the famous Fibonacci series to describe a population dynamic of rabbits, and now, the Fibonacci sequence is used to explain chaos theory, fractals design and even seed developmental pattern in flowers which we see every day. Another mathematician *Daniel Bernoulli* used applied mathematics to study and describe the smallpox effect on the human population [22]. Mathematical modelling allows researchers to explore into complex virtual biological systems and test their predictions which may take years in biological systems but only weeks with the modelling. Mathematical modelling and simulation in cancer research have gained prominence due to the growing importance of mathematics in molecular biology [56]. One of the key points that can be taken from mathematical modeling is that these models are are instrumental to bridge the gap between the understanding of molecular interactions inside and between cells; and what are the potential effects on the tissue level.

Mathematical oncology is a growing field of research where principles

of rate of change, and differential calculus are used to design models and simulations to predict the uncontrolled cell proliferation of cancer cells, and the effects of treatments [43] [34]. According to the data provided by the US National Library of Medicine and the National Institute of Health, the number of publications on the mathematical modeling of cancer is growing exponentially [37]. Mathematical models based on early concept captured the dynamics of cancer growth and the mechanism of proliferation and invasiveness [3]. Based on the biological mechanisms, numerical simulations and mathematical model analysis provide information on evolving population dynamics patterns, which allows studying of complex systems and how any perturbation in these dynamics affects tumor growth or treatment response.

Remarkable advances have been made in the past few decades towards understanding cancer signaling pathways and their dysregulation, leading to the development of tumors. The signaling pathways often exhibit crosstalk with parallel pathways within the cell leading to intertwining complex abnormal activity. Translating patient-specific data into any treatment plan tailored to features of the individual patient's cancer remains the central challenge of personalized medicine. This multifaceted nature of cancer progression often makes it impossible to treat multiple patients with the same treatment regime even when they save the same type of cancer. Moreover, the growth rate of each individual's cancer, the response rate and development of resistance to different rates of therapies could differ. Mathematical modelling can be used to predict and forecast any individual's dynamics based on prior and other data to overcome this problem.

The research work in this thesis aims at the investigation of NMT2 regulation by activating the Akt/mTOR pathway via insulin. Furthermore, this work was conducted to study the dynamics and predicting outcomes in various treatments and conditions at different time points, using mathematical modelling.

2.2 Hypotheses

1. The phosphorylation of NMT2 leads to its translocation to the nucleus of the breast cancer cells resulting in cellular proliferation.

2. Nuclear NMT2 concentration correlates with the IGF1R expression, and cellular proliferation of the breast cancer.

3. The development of a Mathematical Model of breast cancer pathway could be achieved via studying the expression levels of NMT2 and related proteins.

2.3 Objectives

1. To study the NMT2 localization pattern and its effect on cellular proliferation via activating the signaling pathway using insulin.

2. To study the correlation between pNMT2 expression inside the nucleus and the cellular proliferation via studying the IGF1R protein expression.

3. To design and validate a Mathematical Model which can predict the outcomes of various treatments in this pathway by mathematical modelling.

Chapter 3

Mathematical Methods

Mathematical models were designed based on the signaling pathway discussed in the introduction chapter in figure 1.1. In the mathematical models, ordinary differential equations (ODE) were used to explain the dynamics of the pathway. These differential equations were then incorporated in R to develop model simulations. These models were further studied to develop secondary models such as the time-delay model, where certain enzymatic reactions were defined as a time-dependent function.

The models were designed using the Michaelis-Menten Equation to study the phosphorylation and dephosphorylation between the enzyme, substrate and enzyme-substrate complex. The Michaelis-Menten equation, named after *Leonor Michaelis* and *Maud Menten*, is one of the models to study the enzyme kinetics. It gives a correlation between the velocity of the reaction V, the maximum velocity of the reaction V_{max} and the Michaelis-Menten constant K_m. The value of K_m is numerically equal to the substrate concentration at half of the maximum velocity V_{max} of the reaction. The equation is as follows:

$$V = V_{max} \times \frac{[S]}{K_m + [S]}$$

where V is the velocity of the reaction (rate of change of product formation

or the negative rate of change reactant usage); and [S] is the concentration of the substrate. The underlying assumption in Michaelis-Menten equation is that the concentration of the intermediate complex equilibrate very fast on the time-scale of the formation of the product otherwise known as *steady state approximation* i.e., if we assume the enzymatic reaction to be as follows:

$$E + S \underset{k_r}{\overset{k_f}{\rightleftharpoons}} ES \xrightarrow{k_{cat}} E + P$$

where E is enzyme; S is substrate; ES is the enzyme-substrate complex; and P is product, then

$$K_f[E][S] = K_r[ES] + K_{cat}[ES] = (K_r + K_{cat})[ES]$$

and

$$K_m = \frac{K_r + K_{cat}}{K_f}$$

3.1 Model 1: Insulin treatment

In the biological system, starved MCF7 cells were treated with 100nM insulin for 30 minutes, 60 minutes, 360 minutes, and 1440 minutes respectively, and the data collected from this experiment were used to study and investigate the effect of insulin for the insulin treatment mathematical model. To study the dynamics of insulin treated MCF7 cells, the following mathematical model was designed (figure 3.1). This signaling pathway shown in the figure 3.1 is a simplified version of the signaling pathway mentioned in the figure 1.1. Since, we were interested in activating the pathway and how the activation leads to subcellular localization of the protein NMT2; we selected

protein upstream adjacent to NMT2, which is mTOR and to validate the correlation between cellular proliferation to IGF1R protein and IGF1R in the nucleus, we selected IGF1R protein for our mathematical model as state variables. The selected proteins from the mitogenic signaling pathway as state variables in the mathematical model are IGF1R, p-IGF1R, mTOR, p-mTOR, NMT2, cytoplasmic pNMT2, nuclear pNMT2, and nuclear IGF1R (mRNA). Here we investigate the expression of NMT2 in both the cytoplasm and nucleus of the MCF7 cells. The IGF1R pathway is activated here using insulin, which further activates the downstream targets as shown in figure 3.1 and each of those have been assigned a variable to explain the dynamics in the differential equation.

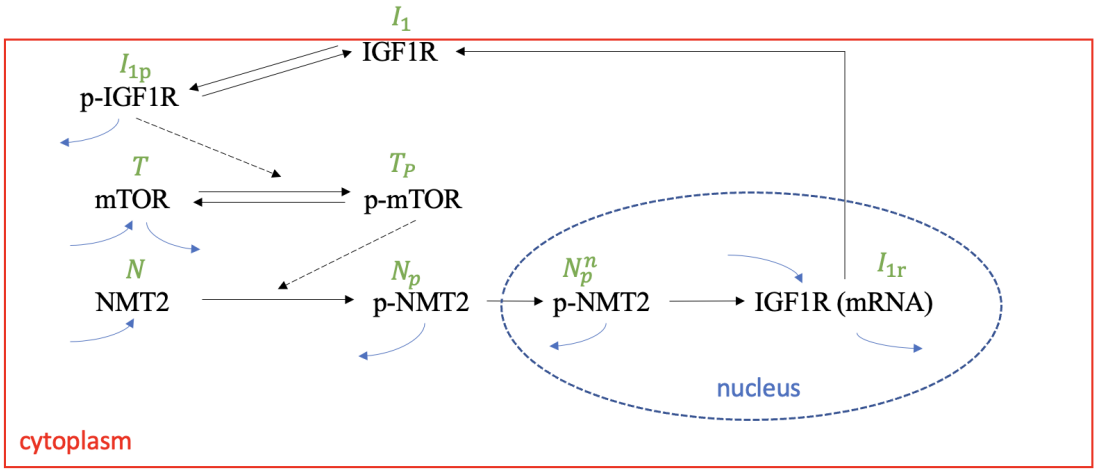

FIGURE 3.1: Base Model 1: Insulin Treatment-Specific downstream targets in the signaling pathway has been considered for this flow diagram. Pathway is activated using insulin leading to the phosphorylation of IGF1R and activating other downstream targets.

The set of state variables and the parameters used in the differential equations to explain the system dynamics are mentioned in the Table 3.1 below.

State variable	Protein	Units
I_1	IGF1R protein	ηmol/L,$p$mol/L
I_{1p}	Phosphorylated IGF1R	ηmol/L,$p$mol/L
I_{1r}	IGF1R (mRNA)	ηmol/L,$p$mol/L
T	mTOR	ηmol/L,$p$mol/L
T_p	Phosphorylated mTOR	ηmol/L,$p$mol/L
N	NMT2 protein	ηmol/L,$p$mol/L
N_p	Cytoplasmic phospho NMT2	ηmol/L,$p$mol/L
N_p^n	Nuclear phospho NMT2	ηmol/L,$p$mol/L
Parameters	**Description**	**Units**
α_X	Catalysis constant for X	$\text{sec}^{-1}, \text{min}^{-1}$
Π	Baseline production constant	ηmol/L,$p$mol/L
π	translation factor	
δ_Y	Degradation factor for Y	
δ	DNA binding factor	
K_Z	Michelis-Menten Constant for Z	ηmol/L,$p$mol/L
μ	scalar factor	

The set of differential equation to explain the dynamics of the pathway in the figure 3.1 are as follows:

$$\frac{dI_1}{dt} = \overbrace{\pi_{I_{1r}} I_{1r}}^{synthesis} + \overbrace{\frac{\alpha_{I_{1p}} I_{1p}}{K_{I_{1p}} + I_{1p}}}^{dephosphorylation} - \overbrace{\frac{\alpha_{I_1} I_1}{K_{I_1} + I_1}}^{phosphorylation} \tag{3.1a}$$

$$\frac{dI_{1p}}{dt} = \overbrace{\frac{\alpha_{I_1} I_1}{K_{I_1} + I_1}}^{phosphorylation} - \overbrace{\frac{\alpha_{I_{1p}} I_{1p}}{K_{I_{1p}} + I_{1p}}}^{dephosphorylation} - \overbrace{\delta_{I_{1p}} I_{1p}}^{degradation} \tag{3.1b}$$

$$\frac{dT}{dt} = \overbrace{\Pi_T}^{baseline} + \overbrace{\frac{\alpha_{T_p} T_p}{K_{T_p} + T_p}}^{dephosphorylation} - \overbrace{\frac{\alpha_T I_{1p} T}{K_T + T}}^{phosphorylation} - \overbrace{\delta_T T}^{degradation} \tag{3.1c}$$

$$\frac{dT_p}{dt} = \overbrace{\frac{\alpha_T I_{1P} T}{K_T + T}}^{phosphorylation} - \overbrace{\frac{\alpha_{T_p} T_p}{K_{T_p} + T_p}}^{dephosphorylation} \tag{3.1d}$$

$$\frac{dN}{dt} = \overbrace{\Pi_N}^{baseline} - \overbrace{\frac{\alpha_N T_p N}{K_N + N}}^{phosphorylation} \tag{3.1e}$$

$$\frac{dN_p}{dt} = \overbrace{\frac{\alpha_N T_p N}{K_N + N}}^{phosphorylation} - \overbrace{\mu N_p}^{nucleus} - \overbrace{\delta_{N_p} N_p}^{degradation} \tag{3.1f}$$

$$\frac{dN_p^n}{dt} = \overbrace{\mu \left[\frac{V_c}{V_n}\right] N_p}^{nucleus} - \overbrace{\delta N_p^n}^{DNAbinding} - \overbrace{\delta_{N_p^n} N_p^n}^{degradation} \tag{3.1g}$$

$$\frac{dI_{1r}}{dt} = \overbrace{\Pi_1}^{baseline} + \delta N_p^n - \overbrace{\delta_{I_{1r}} I_{1r}}^{degradation} \tag{3.1h}$$

where V_c and V_n are the volume of cytoplasm and nucleus of the cells.

In the above set of differential equations π_x [for x belongs to the set of parameters used] denotes the production rate coefficient of the parameter x and δ_y [for y belongs to the same set of parameters] denotes the degradation coefficient of the parameter y respectively.

3.2 Model 2: Control- No Treatment

The mathematical model in figure 3.2 was designed to investigate the expression pattern of NMT2 in cytoplasm and nucleus of MCF7 cells compared to the expression of NMT2 in cytoplasm and nucleus of insulin treated MCF7

cells. The cells were basically starved additionally for the time points 30 min-

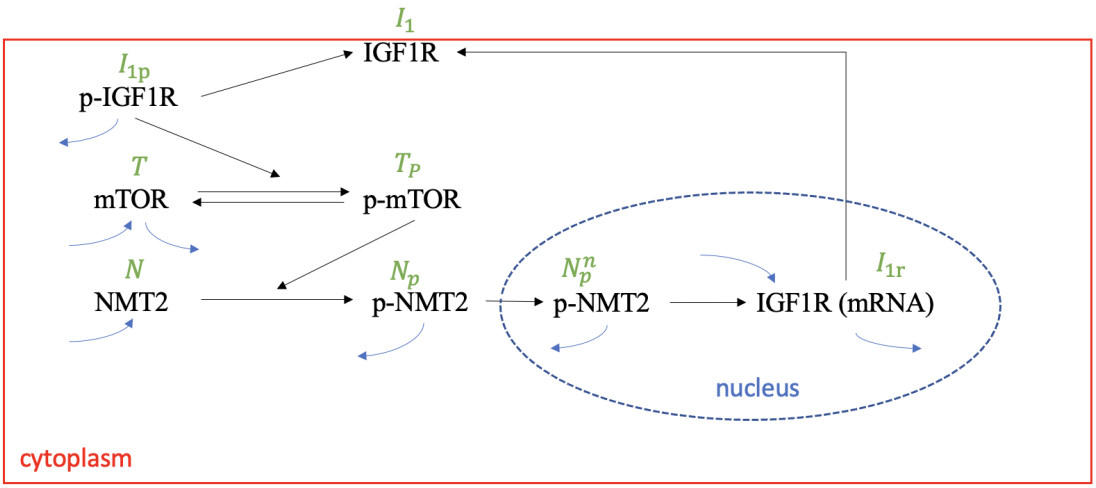

FIGURE 3.2: Base Model 2: Control- No Treatment. Downstream targets in the Akt/mTOR pathway has been considered for this flow diagram. Phosphorylation of IGF1R is absent here because no treatment was given to the MCF7 cells to activate the pathway.

utes, 60 minutes, 360 minutes, and 1440 minutes. Since they weren't treated with any growth factors, we expect minimal phosphorylation of NMT2 and basal expression of IGF1R, which implies the pathway was not activated. It was assumed that the downstream processes still could take place due to the presence of stock proteins in the cells.

The absence of IGF1R phosphorylation has been shown in the differential equation by putting $\alpha_{I_1} = 0$ in the previous set of differential equations for insulin treatment. This changes equation 3.1a and equation 3.1b to equation 3.2a and equation 3.2b, respectively. The set of differential equations explaining the dynamics in the figure 3.2 are as follows:

$$\frac{dI_1}{dt} = \overbrace{\pi_{I_{1r}} I_{1r}}^{synthesis} + \overbrace{\frac{\alpha_{I_{1p}} I_{1p}}{K_{I_{1p}} + I_{1p}}}^{dephosphorylation} \tag{3.2a}$$

$$\frac{dI_{1p}}{dt} = -\overbrace{\frac{\alpha_{I_{1p}} I_{1p}}{K_{I_{1p}} + I_{1p}}}^{dephosphorylation} - \overbrace{\delta_{I_{1p}} I_{1p}}^{degradation} \tag{3.2b}$$

$$\frac{dT}{dt} = \overbrace{\Pi_T}^{baseline} + \overbrace{\frac{\alpha_{T_p} T_p}{K_{T_p} + T_p}}^{dephosphorylation} - \overbrace{\frac{\alpha_T I_{1p} T}{K_T + T}}^{phosphorylation} - \overbrace{\delta_T T}^{degradation} \tag{3.2c}$$

$$\frac{dT_p}{dt} = \overbrace{\frac{\alpha_T I_{1P} T}{K_T + T}}^{phosphorylation} - \overbrace{\frac{\alpha_{T_p} T_p}{K_{T_p} + T_p}}^{dephosphorylation} \tag{3.2d}$$

$$\frac{dN}{dt} = \overbrace{\Pi_N}^{baseline} - \overbrace{\frac{\alpha_N T_p N}{K_N + N}}^{phosphorylation} \tag{3.2e}$$

$$\frac{dN_p}{dt} = \overbrace{\frac{\alpha_N T_p N}{K_N + N}}^{phosphorylation} - \overbrace{\mu N_p}^{nucleus} - \overbrace{\delta_{N_p} N_p}^{degradation} \tag{3.2f}$$

$$\frac{dN_p^n}{dt} = \overbrace{\mu \left[\frac{V_c}{V_n}\right] N_p}^{nucleus} - \delta N_p^n - \overbrace{\delta_{N_p^n} N_p^n}^{degradation} \tag{3.2g}$$

$$\frac{dI_{1r}}{dt} = \overbrace{\Pi_1}^{baseline} + \delta N_p^n - \overbrace{\delta_{I_{1r}} I_{1r}}^{degradation} \tag{3.2h}$$

3.3 Model 3: Rapamycin Treatment

In the rapamycin treatment, the starved cells were treated with 100nM rapamycin at 30 mins, 60 mins, 360 mins, and 1440 mins, respectively. The mathematical model in figure 3.3 was designed to investigate the expression pattern of NMT2 in cytoplasm and nucleus of MCF7 cells compared to the expression of NMT2 in cytoplasm and nucleus of insulin treated and control MCF7 cells.

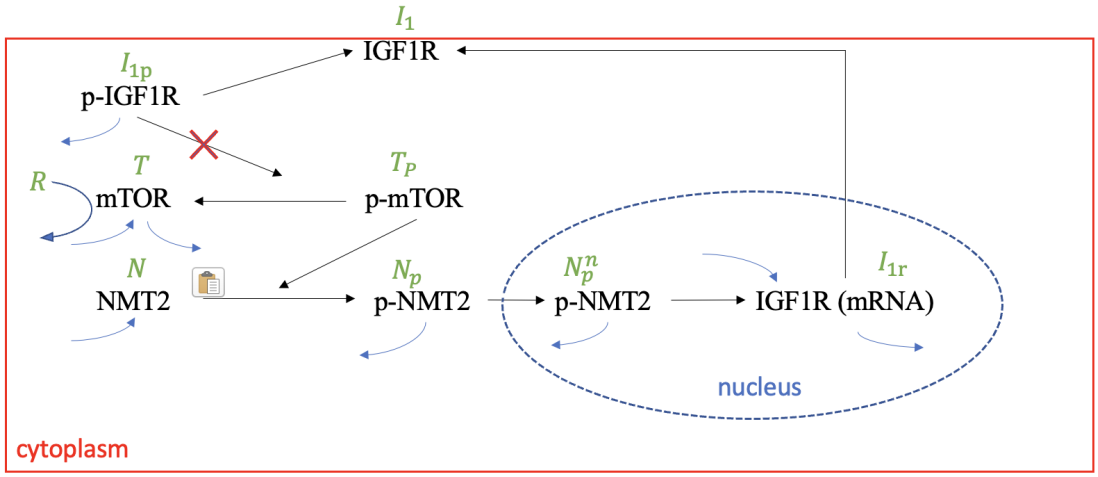

FIGURE 3.3: Base Model 3: Rapamycin Treatment: The cells were treated with 100nM rapamycin which is an inhibitor of mTOR. Two different scenarios are considered for rapamycin effect: strong and weak effect. To incorporate the strong effect of rapamycin in the model, the phosphorylation of mTOR catalyzed by pIGF1R has been inhibited. For the weak effect of rapamycin, the binding of rapamycin to mTOR inhibiting the phosphate group binding domain in mTOR has been considered leading to decrease in phosphorylation of mTOR

Since rapamycin is an inhibitor of mTOR [24, 13], in this model, mTOR inhibition leading to the blocking of mTOR phosphorylation or p-mTOR is shown in two different ways as follows:

3.3.1 Strong effect of Rapamycin

In this case, the phosphorylation of mTOR has been completely blocked by putting the reaction velocity coefficient of mTOR, $\alpha_T = 0$ in the set of differential equations in Base Model 2: Control. By putting $\alpha_T = 0$, the equation 3.2c and the equation 3.2d become equation 3.3a and equation 3.3b, respectively as follows:

$$\frac{dT}{dt} = \overbrace{\Pi_T}^{baseline} + \overbrace{\frac{\alpha_{T_p} T_p}{K_{T_p} + T_p}}^{dephosphorylation} - \overbrace{\delta_T T}^{degradation} \tag{3.3a}$$

$$\frac{dT_p}{dt} = - \overbrace{\frac{\alpha_{T_p} T_p}{K_{T_p} + T_p}}^{dephosphorylation} \tag{3.3b}$$

3.3.2 Weak effect of Rapamycin

In this case, we have assumed that rapamycin forms complexes by binding with mTOR and inhibits phosphorylation of mTOR. To address this change in the mathematical model, we have included a parameter "r" in the equation 3.2c, which denotes the formation of the rapamycin-mTOR complex as follows:

$$\frac{dT}{dt} = \overbrace{\Pi_T}^{baseline} + \overbrace{\frac{\alpha_{T_p} T_p}{K_{T_p} + T_p}}^{dephosphorylation} - \overbrace{\frac{\alpha_T I_{1p} T}{K_T + T}}^{phosphorylation} - \overbrace{rT}^{complex} - \overbrace{\delta_T T}^{degradation} \tag{3.3c}$$

Whereas the equation for the rate of change in the pMTOR concentration remains unchanged to 3.2d which is

$$\frac{dTp}{dt} = \overbrace{\frac{\alpha_T I_{1p} T}{K_T + T}}^{phosphorylation} - \overbrace{\frac{\alpha_{T_p} T_p}{K_{T_p} + T_p}}^{dephosphorylation} \tag{3.3d}$$

3.4 Model Calibration

The dynamics of the signaling pathway is studied using insulin and rapamycin treatments (see figure 3.1, 3.2, 3.3). The models for control and insulin were calibrated using Genetic Algorithm in **R**. The trends observed in the models share similarities to the patterns of experimental data in control and insulin treatment. We see an increase in mTOR with a decrease in p-mTOR in control while the opposite in insulin treatment. Also, we observe lowering nuclear pNMT2 expression in control while increasing in insulin treatment. The model responses supports the regulation of PI3K/Akt/mTOR pathway for NMT2 regulation by p-mTOR in presence of insulin.

In order to calibrate the output of the models to the experimental data, the parametric estimation was done for each parameter involved in each model. The number of parameters is listed above in the list of all state variables and parameters. Out of the 8 state variables, we retrieved experimental data for 4 state variables which are IGF1R protein (I_1), cytoplasmic NMT2 (N), cytoplasmic pNMT2 (N_p), and nuclear pNMT2 (N_p^n). All the experimental data were normalized using β-actin for corresponding time-points. These 4 variables were used to calibrate the models by using residual sum of squares between experimental data and simulated data as follows:

$$\begin{aligned} Error_{global} = &\sum_{i=1}^{T}\sum_{o=1}^{O}(model1_{i,o} - obsInsulin_{i,o})^2 \\ &+ \sum_{i=1}^{T}\sum_{o=1}^{O}(model2_{i,o} - obsControl_{i,o})^2 \end{aligned}$$

where T is the number of time points (30 mins, 60 mins, 360 mins, 1440 mins) and O is the number of observations.

$$\sum_{i=1}^{T}\sum_{o=1}^{O}(model1_{i,o} - obsInsulin_{i,o})^2 = \sum_{i=1}^{T}(I_1(t_i) - \tilde{I_{1,i}})^2 + \sum_{i=1}^{T}(N(t_i) - \tilde{N_i})^2 + \sum_{i=1}^{T}(N_p(t_i) - \tilde{N_{p,i}})^2 + \sum_{i=1}^{T}(N_p^n(t_i) - \tilde{N_{p,i}^n})^2$$

where $\tilde{I_{1,i}}$, $\tilde{N_i}$, $\tilde{N_{p,i}}$, $\tilde{N_{p,i}^n}$ are the observed values for expression of IGF1R, NMT2, pNMT2 and nuclear pNMT2 in insulin treatment respectively. Similarly, in case of control treatment, the model calibration is as follows:

$$\sum_{i=1}^{T}\sum_{o=1}^{O}(model1_{i,o} - obsControl_{i,o})^2 = \sum_{i=1}^{T}(I_1(t_i) - \widetilde{I_{1,i}})^2 + \sum_{i=1}^{T}(N(t_i) - \widetilde{N_i})^2 + \sum_{i=1}^{T}(N_p(t_i) - \widetilde{N_{p,i}})^2 + \sum_{i=1}^{T}(N_p^n(t_i) - \widetilde{N_{p,i}^n})^2$$

where $\widetilde{I_{1,i}}$, $\widetilde{N_i}$, $\widetilde{N_{p,i}}$, $\widetilde{N_{p,i}^n}$ are the observed values for expression of IGF1R, NMT2, pNMT2 and nuclear pNMT2.

We minimized the residual sum of squares between the experimental data and the simulated data to obtain the least error for the best fit using the genetic algorithm and the process was repeated multiple times using R. The plots of each state variable were generated for insulin treatment as well as

TABLE 3.1: State Variables for Plots in the Simulation

Symbol	Protein	Symbol	Protein
I1	IGF1R protein	**I1p**	Phospho-IGF1R
M	mTOR	**Tp**	phospho-mTOR
N	NMT2	**Np**	Cytoplasmic phohpho-NMT2
Npn	Nuclear phospho-NMT2	**I1r**	nuclear IGF1R gene

untreated using R. The state variables used in the plots are mentioned in table 3.1.

The graphs for proteins expression in insulin treated MCF7 cells and untreated MCF7 cells are in figure 5.10 and 5.11 respectively.

Chapter 4

Biological Methods

4.1 MCF7 Cell Culture

MCF7 cells were isolated in 1970 from a 69 year old female cancer patient at the Michigan Cancer Foundation (MCF) where the cell line was established in 1973 for the first time by Herbert Soule and his co-workers [19]. The cell line is positive for the expression of estrogen receptor (ER) and progesterone receptor (PR) [14]. All MCF7 cells were cultured in 100mm cell culture dishes (Griener bio-one) in Dulbecco's modified Eagle medium (DMEM) supplemented with 10% FBS, 1% L-glutamine, 1% streptomycin and 0.3% glucose and kept in the incubator which is set at 37°emperature and 5% CO_2 level for their growth.

MCF7 cells stored in -150°C in freezing media (90% FBS and 10% DMSO) were thawed by keeping the cryovial with the MCF7 cells in the incubator (37°C). The DMSO in the freezing media was washed by mixing 10ml of 10% complete DMEM and then centrifuged for 7-8 minutes at room temperature. The supernatant was decanted keeping the dense pallet in the tube, which then went under vortexing to release the cells, and fresh complete DMEM was added to it and mixed well by pipetting up and down, making single-cell suspension. The mixture was transferred to a clean new 100mm cell culture dish and then kept in the incubator for growth.

4.2 MCF7 Cell Passaging

The MCF7 cells in the cell culture dishes should be at least 80% confluent for passaging. The media in the dish were aspirated out, and the dish was washed with 10ml 1X PBS (room temperature) twice to remove the used media in the dish. Then the PBS was aspirated out, and cells were trypsinized using 1ml 0.25% trypsin-EDTA for 1-2 minutes. Then the trypsin was neutralized by adding 10ml of complete DMEM to the dish, and the mixture was collected in a 50ml falcon tube with 30ml complete DMEM in it. By pipetting up and down the mixture, single cell suspension was made, and the 40ml solution was aliquoted into four new clean 100mm culture dishes for cell growth and kept in the incubator.

4.3 Cytoplasmic-Nuclear Fractionation (CNF)

MCF7 cells were grown in complete Dulbecco's modified Eagle medium (DMEM) (10%) in 16 x 100 mm cell culture plate (Griener bio-one) until they were approximately 90% confluent. The cells were then starved using 10ml starving DMEM media (0.5% FBS, 1% L-glutamine, 1% streptomycin, and 0.3% glucose) for 8 hrs in the incubator. Each 4 out of 16 cell culture plates were treated with 10µl 100 µM insulin, 10µl 100 µm Rapamycin and 10µl di-methyl sulfoxide (DMSO) at four different time points; 30 minutes, 60 minutes, 360 minutes and 1440 minutes making the final concentration 10nM for insulin and rapamycin respectively. Remaining 4 plates were untreated and labelled as controlled for the 4 different time points.

Starving media was decanted and the cells were washed twice with 10ml 1xPBS. Following the PBS wash, 0.5ml of 0.25% trypsin-EDTA (Gibco) was added and left to incubate at 37°C for 1-2 minutes. 10ml complete DMEM was added then and the cells were collected in 15ml falcon tubes (basix, fisher

TABLE 4.1: MCF7 cell count for treatments at various time-points (in million cells/ml)

Treatment-Time Point (hrs)	CNF Replicate 1	CNF Replicate 2
Control 0.5h	5.5	7.2
Control 1h	5.7	4.5
Control 6h	6.0	7.0
Control 24h	5.0	7.0
Insulin 0.5h	5.2	6.5
Insulin 1h	5.0	5.0
Insulin 6h	5.5	6.5
Insulin 24h	7.0	6.5
Rapamycin 0.5h	6.5	6.0
Rapamycin 1h	6.5	5.0
Rapamycin 6h	5.0	5.0
Rapamycin 24h	4.5	5.5
DMSO 0.5h	5.5	6.5
DMSO 1h	6.5	6.5
DMSO 6h	6.2	3.0
DMSO 24h	6.5	5.0

Scientific) and centrifuged for 8 minutes at 3000 rpm at room temperature. The DMEM was decanted and the pelleted cells were resuspended in 1ml 1xPBS. Cell counting was done using hemocytometer then for all the time point treatments which are shown in table 4.1. Approximately 2.0×10^6 cells were collected from the PBS cell solution and transferred to a clean 1.5 ml Eppendorf tube. Cytoplasmic-Nuclear fractionation was conducted according to NE-PER Nuclear Cytoplasmic Extraction Kit protocol (Thermo Scientific). The cytoplasmic extracts and nuclear extracts were then stored in -80°C for future use.

4.4 MCF7 Whole Cell Lysate Collection

MCF7 cells were cultured in Dulbecco's modified Eagle medium (DMEM) supplemented with FBS (10%), penicillin (1%) and streptomycin (1%) in 16x100mm cell culture plates (Griener bio-one) until they were approximately 90% confluent. The cells were starved for 8 hrs overnight in DMEM starving media (0.5% FBS, 1% pen/strap, 1% L-glutamine, 0.3% glucose). Each 4 out of 16 cell culture plates were treated with 10µl of 100 µM insulin, 10µl of 100 µM Rapamycin and 10µl di-methyl sulfoxide (DMSO) at four different time points; 30 minutes, 60 minutes, 360 minutes and 1440 minutes making the final concentration 10nM for insulin and rapamycin respectively. Remaining 4 plates were untreated and labelled as controlled for the 4 different time points.

The media was decanted, and cells were washed twice with 10ml cold 1xPBS. Then 0.5ml ice-cold complete lysis buffer was added to the plates and were placed on ice for 15 minutes. Lysed cells were then scraped from the floor of the plates and pipetted up and down a few times before transferring into clean pre-chilled labelled eppendorf tubes. Then the tubes were centrifuged at 14000 rpm for 7 minutes at 4°C. The supernatant was collected from the tubes to fresh pre-chilled tubes and were stored at -20°C for future use.

4.5 Protein Estimation

Protein concentrations in the whole cell lysates were measured using a bicinchoninic acid (BCA) method of protein estimation (Thermo Scientific) as per manufacturer's instructions. Bovine serum albumin (BSA; 2 mg/ml) was used as a standard. Protein estimation was performed in a 96-well plate (Greiner bio-one). The concentrations of standard BSA were 2000, 1000, 500,

250, 125, 62.5, 31.25, and 15.625 μg/μl. Unknown protein lysates were diluted 2.5-folds (10 μL lysates in a final volume of 25 μl). 200 μL of BCA mixture (reagents A:B, 50:1) was added to all the standards and unknowns, and the plate was placed on a shaker (Sanofi Diagnostics Pasteur) for 30 sec at 150 rpm followed by incubation for 30 min at 37°C. The absorbance was measured at a wavelength of 562 nM using SpectraMax i3 spectrophotometer (Molecular Devices) to determine the concentrations of the proteins.

4.6 Western Blot

Western blot analyses were performed as per the method developed by Towbin (Sambrook). Aliquots corresponding to 25μg of protein were mixed with SDS-PAGE (sodium dodecyl sulfate- polyacrylamide gel electrophoresis) sample buffer and heated on a heating block (Accublock Digital Dry Bath, MBI Equipment) at 95 °C for 5 min.

The samples and a protein ladder, having standard protein of different molecular weights (Precision Plus Protein^{TM} Dual Color Standards, Bio-Rad) were resolved on an SDS-PAGE (10%) and were transferred onto a blotting grade PVDF (polyvinylidene fluoride) membrane (Bio-Rad) that was activated with methanol as per manufacturer's instructions. The membrane was blocked using nonfat dried milk (5%) dissolved in 1x PBST containing tween-20 (0.01%; TBST) for 90 minutes to block the nonspecific sites. The membranes were probed with human NMT2 (monoclonal), human NMT2 (polyclonal) (Sigma Aldrich), Lamin (Sigma Aldrich) and IGF1R (Thermo Scientific) antibodies in 5% milk-PBST, overnight at 4°C. The membranes were washed three times using PBST for 10 minutes each, followed by incubation with appropriate secondary antibody for 90 minutes at room temperature.

The excess was washed with PBST three times for 10 min each. Visualization of the hybridization was carried out using chemiluminescence agent Clarity^{TM} Western ECL Substrate (Bio-Rad) and ChemiDoc XRS molecular imager (Bio-Rad).

4.7 Trypan Blue Proliferation Assay

MCF7 cells were cultured in Dulbecco's modified Eagle medium (DMEM) supplemented with FBS (10%), penicillin (1%) and streptomycin (1%) in sixteen 100mm cell culture plates (Griener bio-one) until they were approximately 90% confluent. The cells were treated with 100nM insulin, 100nM rapamycin and equal amounts of DMSO to rapamycin separately for 0.5h, 1h, 6h, and 24h time points. At the respective time point the medium was siphoned off and the cells were washed with 1X PBS and then trypsinized with 1mL 0.25% Trypsin-EDTA (Gibco) for one minute at 37°C to detach the adhered cells. The trypsin was neutralized by adding 10mL complete DMEM to the cells and then they were collected in a 15mL falcon tube for centrifugation. After that, the supernatant was decanted, leaving the pallet at the bottom which was loosened by vortexing. 1mL of fresh complete-media was added to the cells and mixed very well. An aliquot of the sample was collected in a small microcentrifuge tube and was stained with 1 volume of 0.4% trypan blue (Gibco) and placed onto a hemocytometer (Bright-line). The living cells which did not pick up the stain were counted manually under a light microscope (Leitz Wetzlar).

4.8 Crystal Violet Proliferation Assay

Approximately 25000 MCF7 cells were seeded in two rows of eight 96 well plates for 0.5h, 1h, 6h, 24h, 48h, 72h, 96h, and 120h time-points for various

treatments (control, insulin, rapamycin and DMSO) and allowed to adhere for 24h in a 5% CO_2 incubator maintained at 37°C before the treatments. The final concentration of 100nM insulin and rapamycin were used for the treatments and DMSO was in equal amounts to that of rapamycin were used for DMSO treatment. After the treatments, at the respective time-points, the medium was siphoned off by putting the plate upside down on a paper towel. After the media was out of the plate, 50μl of 0.5% crystal violet was added to each of the two rows of the well and incubated for 20 min at room temperature with slight agitation. Excess crystal violet was then washed away by immersing the plate in distilled water in a 1000ml beaker three times. The water was changed between each wash. The plate was dried by putting the plate upside down on a paper towel allowing excess water to run off. The plate was kept for 16h then at room temperature to be completely dry and then 200μL of methanol was added to each well to solubilize the crystal violet stain. The plate was agitated in the orbital shaker at 20rpm for 20 minutes until the crystal violet was uniform with no areas of dense coloration in the bottom of the wells. The absorbance was measured at a wavelength of 570 nM using a SpectraMax i3 spectrophotometer (Molecular Devices) and the results are as follows:

TABLE 4.2: Crystal Violet Proliferation Assay: Absorbance values for different treatments at various time-points (570nM)

Time-Points (hrs)	**Control**	**Insulin**	**Rapamycin**	**DMSO**
0.5	1.90465	1.88663	1.4949	1.59257
1.0	1.90445	1.86007	1.70628	1.85207
6.0	1.9438	1.94503	1.40771	1.41148
24.0	2.41345	2.80513	1.08651	1.40378
48.0	2.67588	2.86375	0.72493	1.21687
72.0	3.36228	3.37847	0.7476	1.37428
96.0	3.05413	3.30277	0.52985	1.0364
120.0	2.49198	1.3109	0.62958	1.0073

WT MCF7 cells with approximately 90% confluency (around 1.5×10^6)

treated with 100 nM rapamycin, and DMSO for 0.5h, 1h, 6h, and 24h. RNA was extracted using E.Z.N.

Chapter 5

Results

5.1 Crystal Violet Proliferation Assays

Cellular Proliferation rates for MCF7 cells with or without insulin treatment for 0.5h, 1h, 6h, 24h, and 48h time points were studied. The wells were seeded with 25000 MCF7 cells and were treated with 100nM insulin, 100nM rapamycin or DMSO in triplicate wells.

The crystal violet assay is triarylmethane dye that relies on the amount of cell biomass rather than the number of cells, as the dye binds to ribose sugar such as DNA in nuclei. The assay was performed in 96 well plates with approximately 25000 MCF7 cells in each well for all the treatments. The initial reading was done at 0.5h after the treatments for the 0.5h time point.

The absorbance is representative of the number of cells. There was an increased cell proliferation with time. Insulin treatment displayed a higher proliferation rate of MCF7 cells than no treatment (control). The increased proliferation of MCF7 cells due to the insulin treatment is attributed to the activation of the insulin and insulin like growth factor pathway. There was a gradual decrease in the MCF7 cells treated with DMSO or rapamycin. DMSO was used as a vehicle control for the rapamycin treatment. The decrease in proliferation due to DMSO treatment has been observed previously (ref). i=In this case, I compared the change in proliferation due to rapamycin treatment to that of DMSO. Rapamycin is an inhibitor of mTOR the downstream

target of insulin pathway. The rapamycin treatment was expected to show reduced cell proliferation compared to DMSO or treatment with or without insulin. By 120h the insulin treatment led to a decline in absorbance. The decrease in absorbance was due to the cell death as the rapid proliferation of cells due to insulin treatment took over all the space available and then started coming off the well due to insufficient well space.

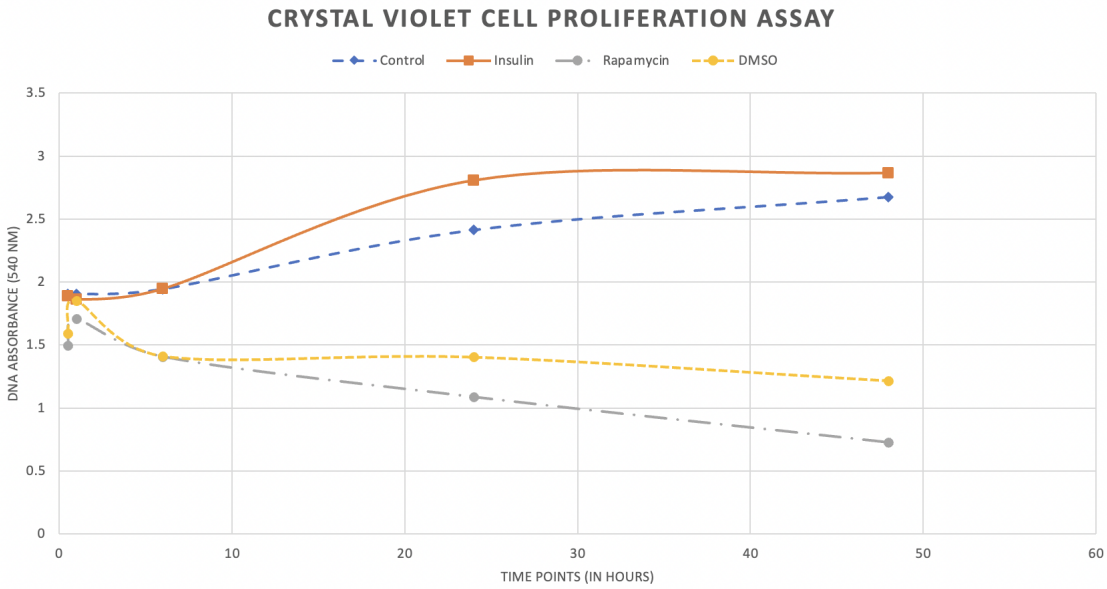

FIGURE 5.1: Crystal Violet assay of cellular proliferation rate of MCF7 cells with different treatments. Each point is an average of six biological replicates.

5.2 NMT2 and phospho-NMT2 expression

From the cytoplasmic-nuclear fractionation of MCF7 cells treated with 100nM insulin, 100nM rapamycin or DMSO at different time points, the cytoplasmic protein and nuclear protein samples were collected, and the mixture samples were prepared according to the calculations in table 5.1 such that protein concentration for Western blot was same (25 μg) when loaded on the gel for SDS-PAGE. Western blot was performed to investigate the NMT2 and pNMT2 protein expression in those samples. Figure 5.2, figure 5.3, figure 5.4,

and figure 5.5 shows the NMT2 and pNMT2 protein expression at 0.5h, 1h, 6h and 24h time points.

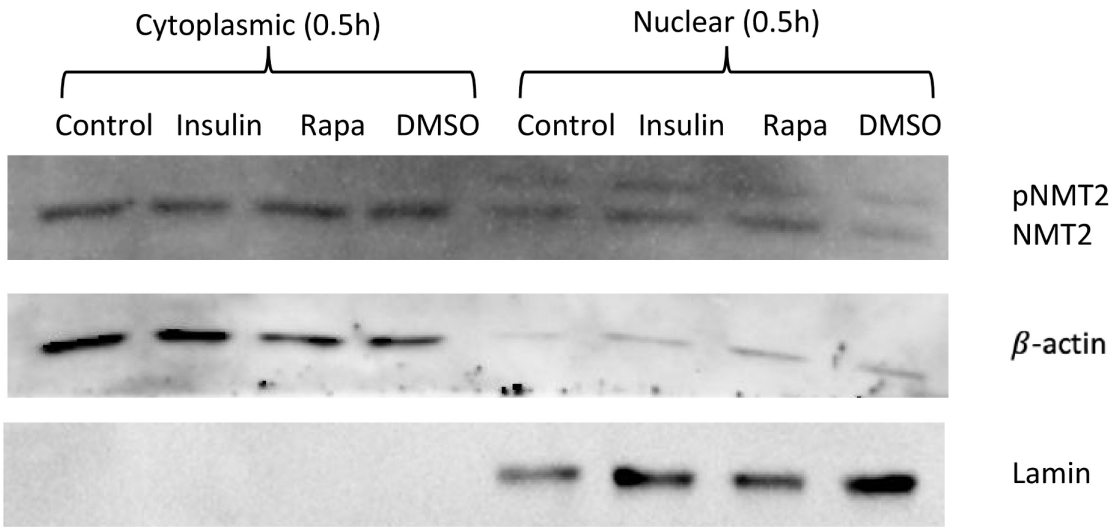

FIGURE 5.2: Western Blot analysis of the Cytoplasmic and the Nuclear protein expression of NMT2 and pNMT2 in MCF7 cells starved for 7h in serum-deprived media followed by treatments with Insulin, Rapamycin, and DMSO for 30 minutes. Volume corresponding to 25μg of protein was separated on SDS-PAGE and Western blot analysis was carried out as described in the Biological Methods section.PVDF membrane was probed with primary anti-NMT2 monoclonal antibody (Mouse, Sigma) and HRP conjugated Goat-Anti-Mouse secondary antibody and visualization of the hybrid was carried using ChemiDoc XRS molecular Imager (Bio-rad). The membrane was then stripped and re-probed with β-actin and then lamin.

A 60 kDa band corresponding to endogenous NMT2 was observed for all the treatments. Also, a band just above the 60 kDa band was observed in nuclear proteins corresponding to phospho-NMT2. Anti-β-actin antibody was used as a loading control, and anti-lamin was used to check the purity of cytoplasmic and nuclear fractions from the fractionation of MCF7 cells.

At 30 minutes time-point (Fig 5.2), low intensity bands for pNMT2 in the nucleus for all the treatments and control were observed. Although the bands are faint overall, but the band intensity is high for insulin treatment compared to the band intensity in control. As the time progressed, the pNMT2 bands got denser for both the control and the insulin treatment. However

TABLE 5.1: MCF7 cytoplasmic and nuclear fraction protein concentration

Fraction	Sample	Concentration(mg/mL)
Cytoplasm	Control 0.5h	1.964
Cytoplasm	Control 1.0h	2.236
Cytoplasm	Control 6.0h	2.402
Cytoplasm	Control 24h	2.513
Cytoplasm	Insulin 0.5h	2.325
Cytoplasm	Insulin 1.0h	3.128
Cytoplasm	Insulin 6.0h	2.142
Cytoplasm	Insulin 24h	2.315
Cytoplasm	Rapamycin 0.5h	2.058
Cytoplasm	Rapamycin 1.0h	2.367
Cytoplasm	Rapamycin 6.0h	1.871
Cytoplasm	Rapamycin 24h	2.042
Cytoplasm	DMSO 0.5h	2.036
Cytoplasm	DMSO 1.0h	3.194
Cytoplasm	DMSO 6.0h	2.361
Cytoplasm	DMSO 24h	2.034
Nuclear	Control 0.5h	0.757
Nuclear	Control 1.0h	0.822
Nuclear	Control 6.0h	0.758
Nuclear	Control 24h	0.861
Nuclear	Insulin 0.5h	0.886
Nuclear	Insulin 1.0h	1.105
Nuclear	Insulin 6.0h	0.972
Nuclear	Insulin 24h	1.056
Nuclear	Rapamycin 0.5h	0.860
Nuclear	Rapamycin 1.0h	0.739
Nuclear	Rapamycin 6.0h	1.147
Nuclear	Rapamycin 24h	0.895
Nuclear	DMSO 0.5h	0.838
Nuclear	DMSO 1.0h	0.755
Nuclear	DMSO 6.0h	0.910
Nuclear	DMSO 24h	0.723

the band intensity of insulin treatment remains higher indicating an increasing rate of translocation of pNMT2 in the nucleus with time. At 1 hour time-point (Fig 5.3), a 9-fold higher expression of pNMT2 in the nucleus compared to the 0.5h time-point. Interestingly, at 1 hr time point, the nuclear pNMT2 expression remains higher for the insulin treatment compared to the control. A 2-fold increase in NMT2 band intensity in the cytoplasm was observed for the insulin treatment and the control compared to that of the 0.5 h time-point.

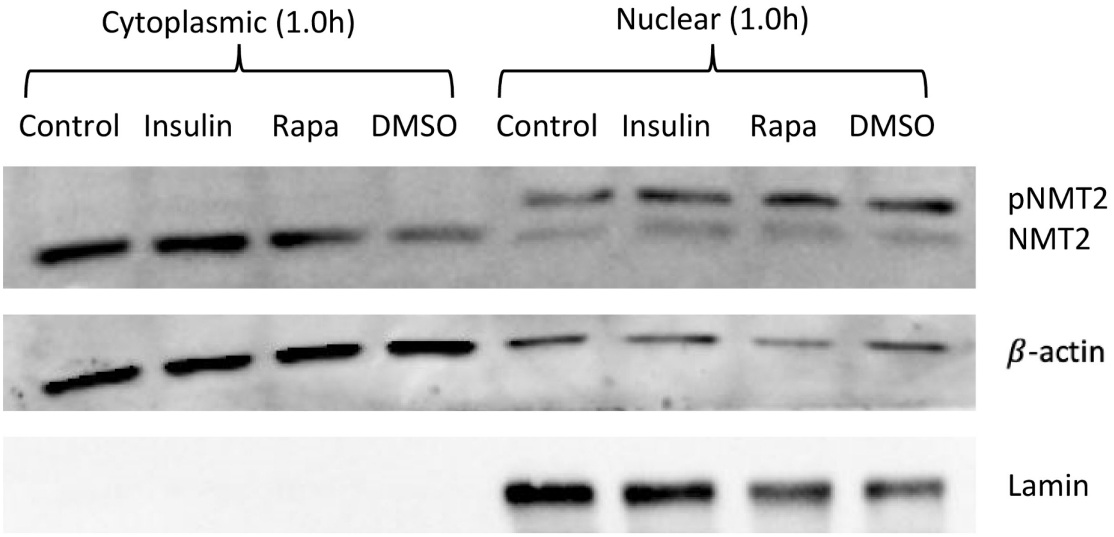

FIGURE 5.3: Western Blot image of the Cytoplasmic and the Nuclear protein expression of NMT2 and pNMT2 in MCF7 treated with Insulin, Rapamycin, and DMSO for 1 hour. 25μg of protein loaded for each sample. PVDF membrane was probed with primary anti-NMT2 monoclonal antibody (Mouse, Sigma) and HRP conjugated Goat-Anti-Mouse secondary antibody and visualization of the hybrid was carried using Chemi-Doc XRS molecular Imager (Bio-rad).

The NMT2 expression in the figure 5.3 potentially indicate the beginning of an exponential increase in the rate of pNMT2 translocation to the nucleus which is confirmed by the 6 hr time-point in the figure 5.4. The band intensity for pNMT2 has increased approximately thirty-fold for the 6 hr time-point with respect to 30 minutes time-point suggesting an increase in NMT2 phosphorylation and translocation to the nucleus. This was mirrored by the concomitant decrease in cytoplasmic NMT2 expression level in 6hr time-point

(fig 5.4), suggesting that cytoplasmic NMT2 is getting phosphorylated and translocated to the nucleus.

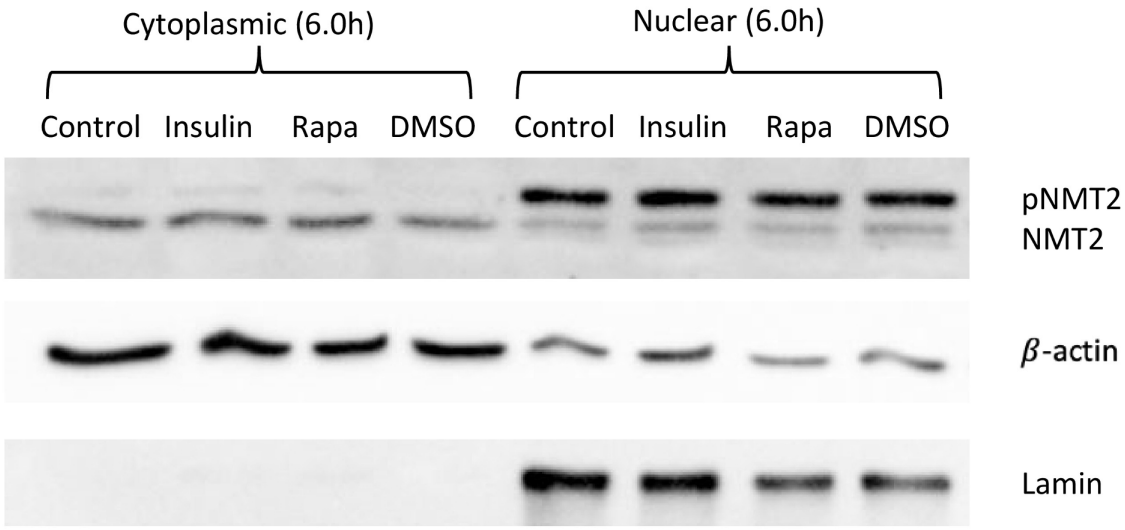

FIGURE 5.4: Western Blot image of the Cytoplasmic and the Nuclear protein expression of NMT2 and pNMT2 in MCF7 treated with Insulin, Rapamycin, and DMSO for 6 hours. 25μg of protein loaded for each sample. PVDF membrane was probed with primary anti-NMT2 monoclonal antibody (Mouse, Sigma) and HRP conjugated Goat-Anti-Mouse secondary antibody and visualization of the hybrid was carried using Chemi-Doc XRS molecular Imager (Bio-rad).

In figure 5.5, the expression pattern for pNMT2 is depicted 24 hours. The relative nuclear pNMT2 expression doesn't vary significantly for both control and insulin treated MCF7 cells. A similar pattern is also observed in the cytoplasmic NMT2 expression in both control and insulin treatment.

The figure 5.6 shows the relative pNMT2 expression pattern with time. The nuclear pNMT2 bands in figure 5.2, figure 5.3, figure 5.4, and in figure 5.5 were quantified using the Image Lab software. The values were normalized by dividing the nuclear pNMT2 value by the respective nuclear total NMT2 value. Then taking Control 0.5h as the reference frame, fold increase/ decrease was calculated for other values as well. All the pNMT2/NMT2 values were divided with pNMT2/NMT2 value of control at 0.5h to make Control 0.5h as the reference frame.

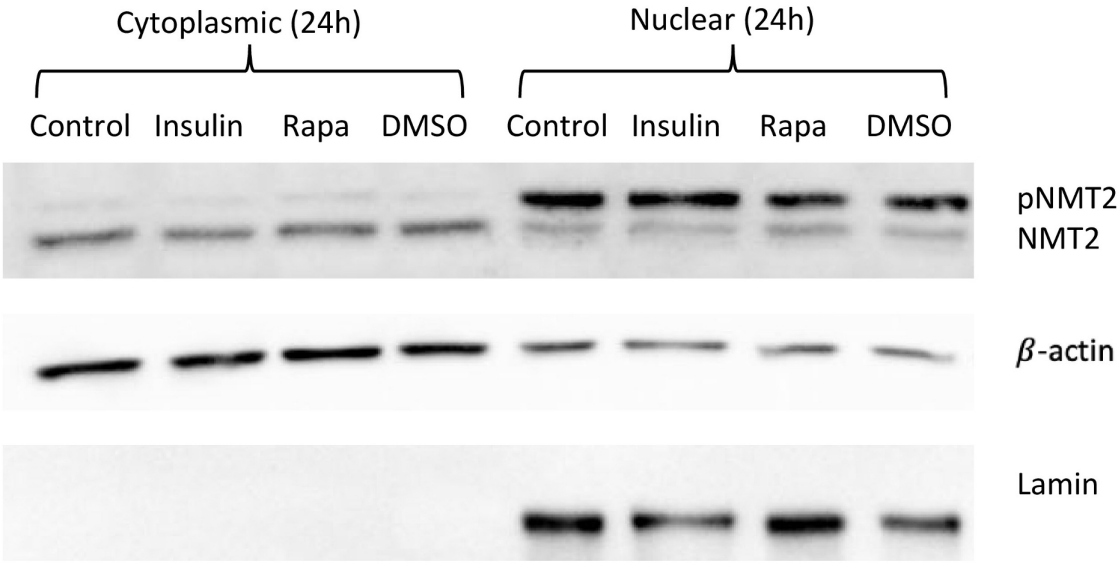

FIGURE 5.5: Western Blot image of the Cytoplasmic and the Nuclear protein expression of NMT2 and pNMT2 in MCF7 treated with Insulin, Rapamycin, and DMSO for 24 hours. 25μg of protein loaded for each sample. PVDF membrane was probed with primary anti-NMT2 monoclonal antibody (Mouse, Sigma) and HRP conjugated Goat-Anti-Mouse secondary antibody and visualization of the hybrid was carried using Chemi-Doc XRS molecular Imager (Bio-rad).

Since the focus of the experiment was to observe the NMT2 and phospho NMT2 protein expression, we were interested in investigating the expression patterns of the mentioned proteins in an activated mitogenic pathway in MCF7 cells using insulin compared to MCF7 cells without treatment. So, the figure 5.6 shows the phospho NMT2 expression in control and insulin treated MCF7 cells for indicated time points. To visualize the protein expression for rapamycin treatment, a curve was also generated from the data obtained from the experiments (table B.2 and table B.3) and is available in the appendix figure B.1. In the figure B.1 we can see that the pNMT2 expression in rapamycin treated MCF7 cells starts declining after 6h time point. Since, rapamycin is an inhibitor of mTOR inhibiting the downstream signalling, the pNMT2 expression is declining. The time delay for the inhibition might suggests the delay in the effect of rapamycin on the entire MCF7 population.

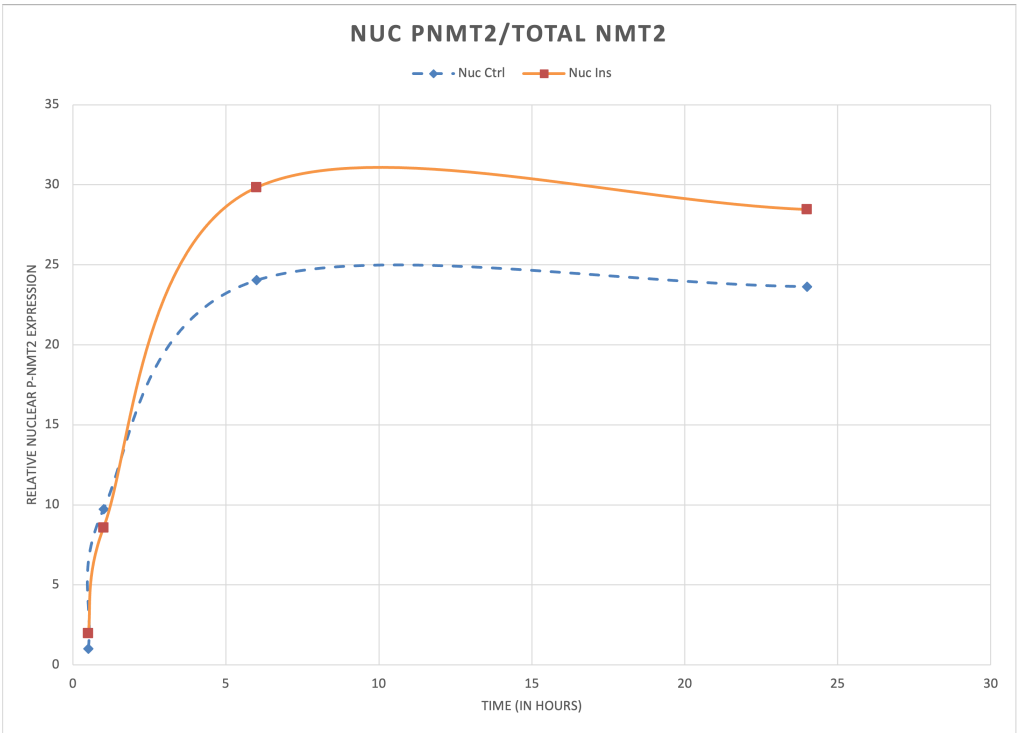

FIGURE 5.6: Relative Nuclear pNMT2 expression for Control and Insulin treated MCF7 cells. The fold increase/decrease values were calculated by fixing the Control 0.5h value as 1.

Since new cells are being formed, there might be a delay in the effect of rapamycin. We can see this delay in the proliferation assay as well where we see in increasing rate of cell proliferation in rapamycin treated MCF7 cells until 1h time point in the figure 5.1.

5.3 IGF1R protein expression

Dysregulation of the PI3K/Akt/mTOR pathway has been implicated in the development and progression of many types of cancer including ER+ breast cancer [18]. IGF1R is one of the receptor tyrosine kinase transmembrane receptors responsible for the activating this pathway. Whole cell lysates of MCF7 wild type cells for control, treated with 100nM insulin, 100nM rapamycin or DMSO at 0.5hr, 1hr, 6hrs and 24 hrs were collected. IGF1R protein expression levels for all the samples were determined by Western blot analysis which are shown in the figures 5.7 and 5.8.

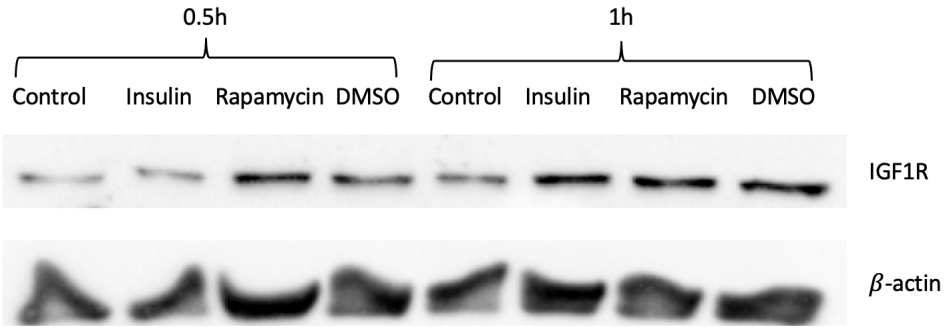

FIGURE 5.7: IGF1R for Control, Insulin, Rapamycin, DMSO at 0.5h and 1h

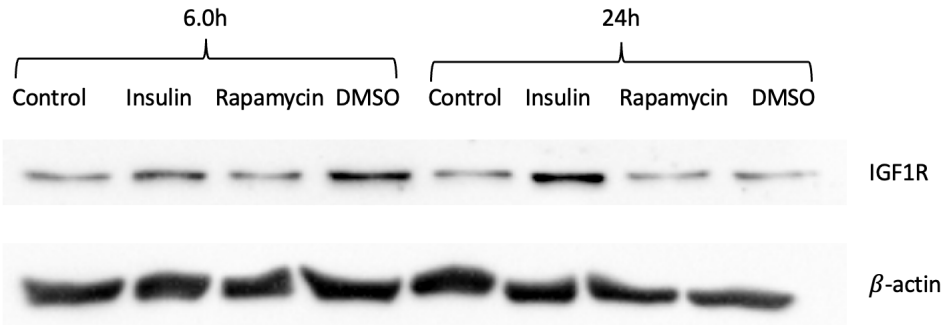

FIGURE 5.8: IGF1R for Control, Insulin, Rapamycin, and DMSO at 6.0h and 24h

The Western blot analysis shows a very faint band of IGF1R protein at the

0.5h time-point for both control and insulin treated MCF7 cells with increasing band intensity over time. At each time point, insulin-treated MCF7 cells shows a higher band intensity, suggesting higher IGF1R protein expression than control. This result suggests that activation of the insulin growth factor pathway leads to an increase in IGF1R protein expression over time. It is evident from the figure 5.1 that there is an increase in cellular proliferation over time, suggesting that IGF1R expression in directly proportional to the rate of cellular proliferation, which has previously been reported [45, 41].

Image Lab 6.0 protein expression analysis software was used for the quantitative analysis of the expression of the IGF1R polypeptide bands and constructed the graph in figure 5.9 below. The software normalized the expression of IGF1R protein by dividing the protein expression intensity by the expression intensity of β-actin, a cellular housekeeping protein constitutively expressed in mammalian cells. Insulin treated cells express high IGF1R protein expression which increases over time, whereas in the case of control, it diminishes after 6 hr time point.

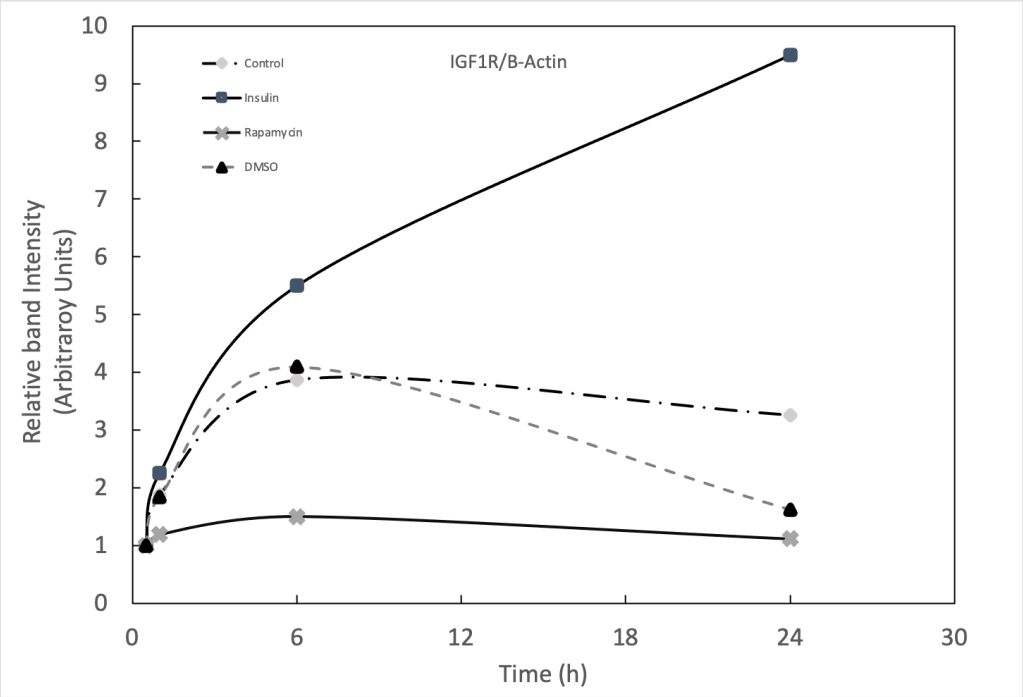

FIGURE 5.9: Normalized IGF1R protein expression levels against β-actin for control, insulin, rapamycin and DMSO treatment at 0.5h, 1h, 6h and 24h.

5.4 Simulation

Using genetic algorithm in R, the model was calibrated, and the values of the parameters in the system of differential equations were generated. Afterward, qualitative analysis refined those parametric values to have a better fit, and simulations for the state variable (proteins) dynamics were developed for control treatment, and insulin treated mathematical model. The simulations are as follows in the figures 5.10 and 5.11.

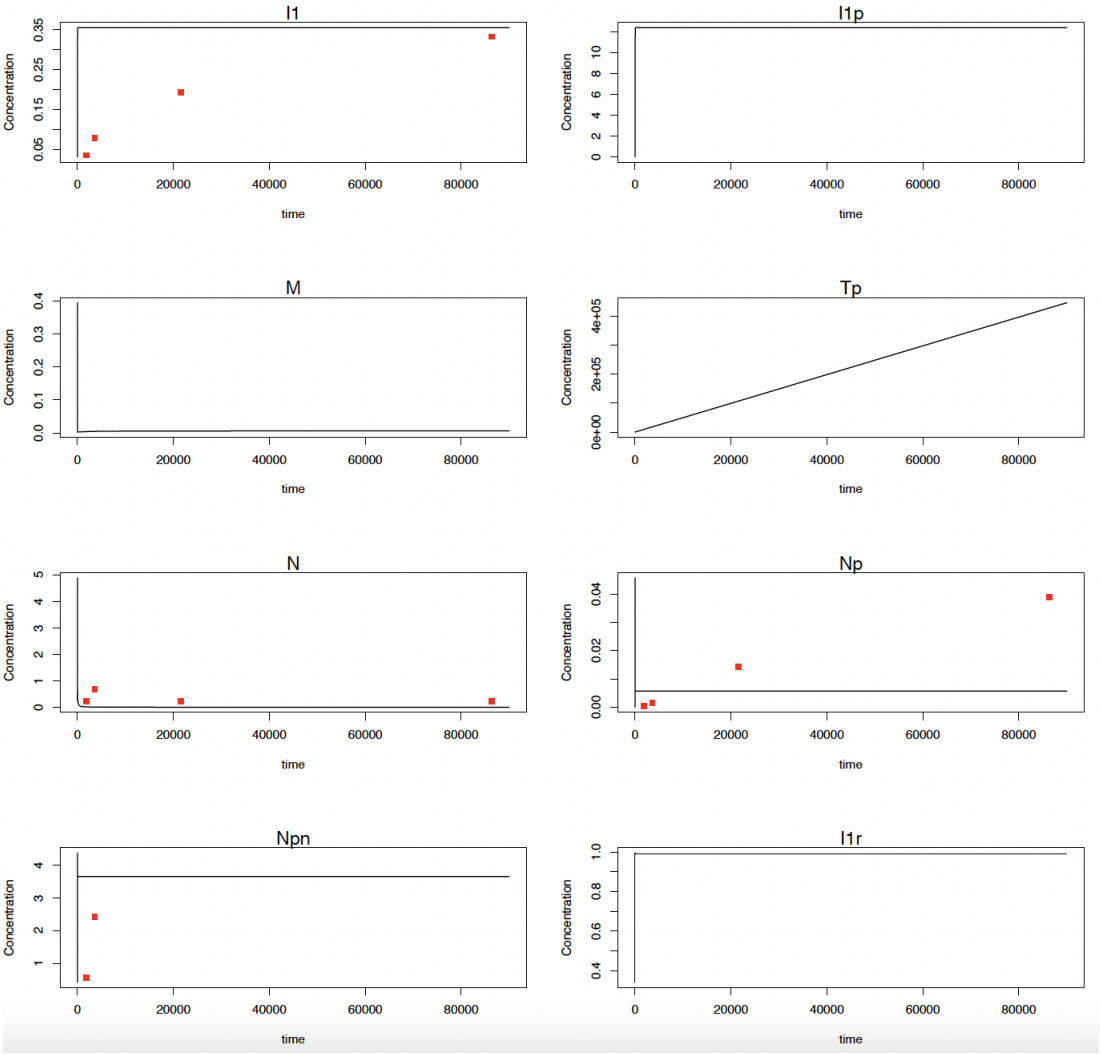

FIGURE 5.10: Plot generated for Insulin treated MCF7 model using R for the eight state variables mentioned in the table 3.1. These eight variables are the target proteins in the IGF pathway which are considered for the mathematical modelling. The plot predicts the expression pattern of the proteins over a time period of 24 hours. The red dots represent the protein expression data collected from biological experiment for the corresponding variables.

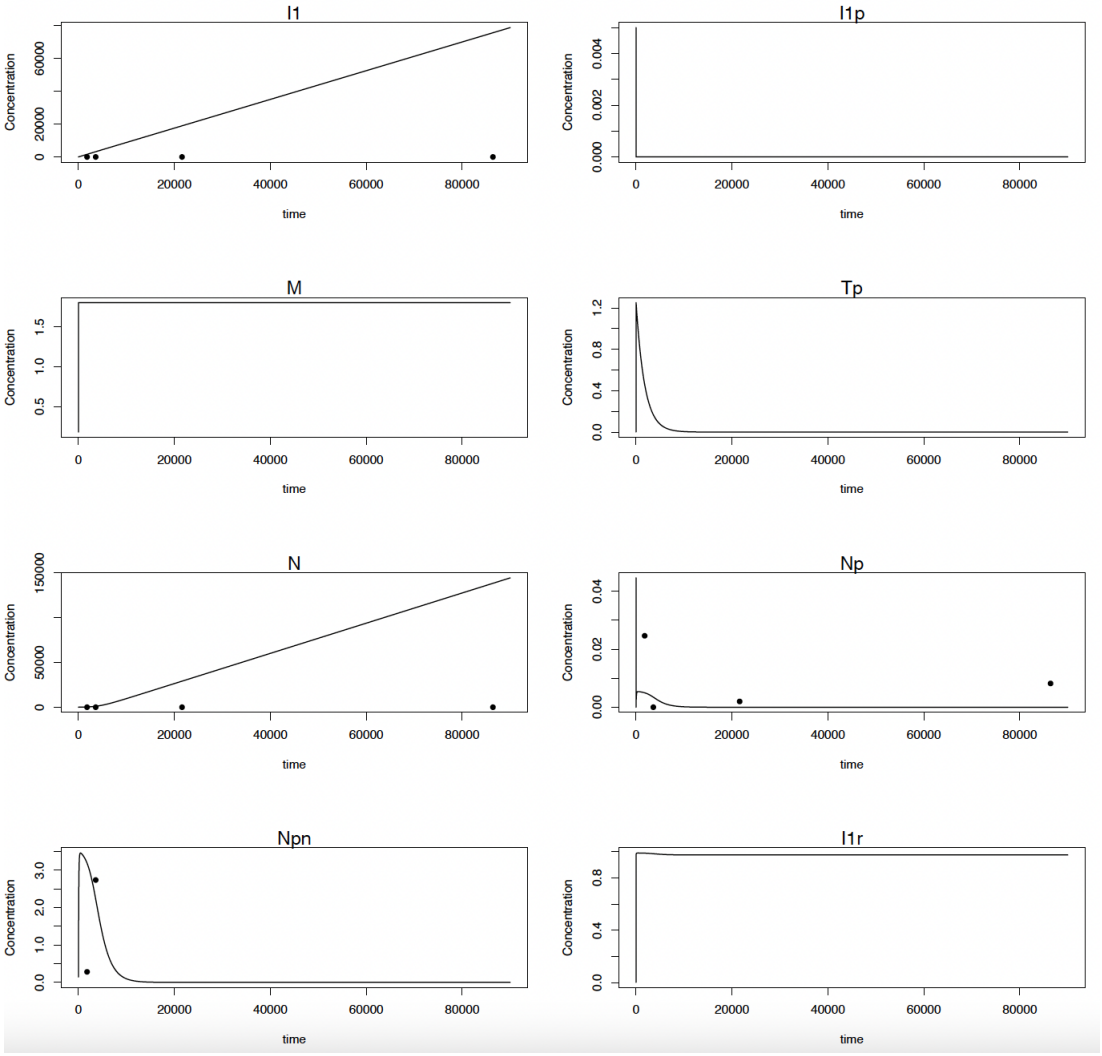

FIGURE 5.11: Plot generated for untreated MCF7 model using R for the eight state variables mentioned in the table 3.1. These eight variables are the target proteins in the IGF pathway which are considered for the mathematical modelling. The plot predicts the expression pattern of the proteins over a time period of 24 hours. The black dots represent the protein expression data collected from biological experiment for the corresponding variables.

Chapter 6

Discussion

Association of NMT has been found in several studies, but it is yet to discover the exact role of NMT even with very little details on its regulatory mechanism [35, 31]. In this thesis, we have shown the translocation of the NMT2 pattern when phosphorylated using insulin and have designed a mathematical modelling to simulate the dynamics within the cell for numerous conditions. Post-translational modifications, including phosphorylation have been established to regulate the activity and interactions of proteins in our body, with phosphorylation as the most utilized process by eukaryotic cells for protein regulation [25, 21, 36].

NMT1 and NMT2 share 77% amino acid sequence homology, and in our lab, it has been demonstrated that NMT1 and NMT2 can be phosphorylated by a Serine/Threonine kinase mTOR which is a hub in many cell-signaling pathways and one of the key players in insulin like growth factor (IGF) pathway. Over-expression of NMT is correlated with the progression of several types of cancer such as colorectal cancer and brain cancer although the exact role of it is yet to be discovered [6, 50].

To determine whether the phosphorylation of NMT2 protein plays any role in cellular proliferation, a crystal violet proliferation assay was performed over the period of 120 hours. The IGF pathway was activated using insulin, and the results were compared against that of the untreated MCF7 cells. We

see that the cellular proliferation rate is higher in insulin than the control (untreated), and after the 6 hr time-point, the rate increases two-fold in insulin treated cells at 24h time point. Since, the cells were seeded in a 96 well-plate, the cells started to cover the space and the rate of proliferation started getting to homeostasis phase and after 96 hr we see a steep decline in its rate due to cell death due to lack of space and nutrition. In the control line, the rate of proliferation is increasing very uniformly.

The nuclear pNMT2 (normalized) potentially reached a steady-state at 6 h time-point after a gradual increase from 0.5 to 1 h time-point. The increased nuclear localization of pNMT2 prior to extensive cell proliferation indicates that the nuclear pNMT2 triggers mitogenic genes and consequently activates mitogenic pathways for cellular proliferartion. Earlier, our group demonstrated direct correlation with pNMT2 mimic and IGF1R expression. Previous studies in our lab employing site-directed mutagenesis have shown that NMT2, upon phosphorylation, tends to translocate inside the nucleus of the cells. This suggests the direct proportionality between nuclear pNMT2 and cellular proliferation. Hence, it is plausible that pNMT2 may play a role in the transcriptional regulation of mitogenic genes and thus, leading to cellular proliferation.

The dysregulation of the Akt/mTOR cell proliferation pathway has been associated with the progression and development of various cancers such as colorectal cancer and pancreatic cancer. The aberrant expression of NMT protein has been found to be related to this dysregulation [6, 27]. Understanding the connection between this pathway and NMT has been widely focused on in our lab and previous work has established a relationship between NMT1 and mTOR kinase, which is a member of the insulin like growth factor (IGF) pathway. IGF1R protein is one of the key regulating proteins of the pathway, upon activation of which leads to activation of all the downstream proteins and increased expression of it could result in increased cellular proliferation.

A study has already shown increased IGF1R expression as the hallmark feature of breast cancer [45].

To determine the expression of IGF1R protein in MCF7 breast cancer cells, Western blot was performed for untreated, insulin treated, rapamycin treated or DMSO treated MCF7 cells probed with IGF1R antibody (figure 5.9). The resulting band values were quantified and normalized by dividing those with corresponding β-actin antibody band values. Insulin treated breast cancer cells shows an increased IGF1R expression with time whereas IGF1R protein expression in untreated cells diminishes slowly after 6 hour time point with time. Rapamycin inhibits mTOR from being phosphorylated by binding to it and prevents the activation of downstream targets leading to attenuating the cellular proliferation. I observed low IGF1R protein expression in rapamycin treated MCF7 cells. Correlating the IGF1R expression data with crystal violet assay for cellular proliferation, we could argue that IGF1R protein is a biomarker for cell proliferation.

With the rising numbers in breast cancer cases among Canadian women, the government has introduced several policies to ensure the awareness that discovery of any lump related to breast tissue to be taken very seriously so that the diagnosis could be done in an early stage. Upon early detection of cancer subtype, the treatment regimen could be developed easily for the patient. Almost all breast cancer patients undergo surgery and radiation therapy to remove the bulk of the cancerous tissue. Conventionally, adjuvant therapy is followed to help prevent the relapsing and growth of any residual cancer cells which depend on the subtype of the cancer. Approximately 70% of all breast cancer cases are ER+ and out of those, 50% express denovo resistance to the therapy. Even though the treatment schemas follow the policies, the resistance continues to be a problem due to which there is urgency of applying new changes to the policies governing the treatment schemas to increase the survival rates of the patients.

The mathematical models and the associated results discussed in this thesis shows the expression pattern of cytoplasmic and nuclear NMT2 protein as well as other proteins involved in the IGF pathway in various conditions can serve as a tool for better approximation to define the treatment schema. In ER+ breast cancer cells, nuclear NMT2 appears to cause an increase in cellular proliferation rate. Hence, the NMT protein status in the tissue biopsy process could be beneficial.

The average cost for breast cancer treatment has gone up more than two folds from $15000 to $35000 for younger patients and $13000 to $29000 for older patients over the last decade recorded in Ontario, Canada whereas the average undiscounted cost of treating Canadian women with breast cancer varies by $23000 per case for stage I to $36000 per case for stage IV [9, 7]. Even though Canadian universal health care system covers for most of the charges, there is a lifetime cap on the insurance. The reason for the increased cost is due to more patients receiving the adjuvant therapy to keep cancer from returning. Introduction of policy change towards addition of biopsy might increase the price initially but in the long run it would save a large amount of time during the treatment which would have cost even more. The secondary costs involving repeat surgeries due to relapses could be avoided with the introduction of new policy changes and thus help avoid the cost that comes with these. So, considering all the scenario, the long run outcome would save individuals from a burden of cost and the healthcare system would be benefited economically as well as in terms of time.

The endgame of all the research is to make the lives of common people better in terms of health and it all comes down to drug designing at the end. The data collected during my tenure could be used to develop not only new therapeutic drugs but also, the mathematical models could be used to design software and apps to approximate the protein status in breast cancer patients. The models open doors for improvement with more experimental data and

also could be adjusted to various experimental conditions. Previous studies from our lab has demonstrated nuclear NMT2 as a predictor of poor prognosis and recurrence. So breast cancer patients showing tumor with nuclear NMT2 could be put on surveillance for a frequent diagnostic procedures for better outcome.

Chapter 7

Conclusion

Millions of women are getting diagnosed with breast cancer worldwide every year with a significant chance of developing resistance to first line endocrine therapies which decrease the survival rate [59]. The discovery of potential biomarkers and novel therapeutic targets are in urgency. I believe the results from this study might contribute towards the solution to the current problems in breast cancer diagnosis and treatment. This thesis has shed light on the investigation of the PI3K/Akt/mTOR pathway and its correlation with NMT2 translocation in ER+ breast cancer cells using experimental data and mathematical modelling using the data. It may contribute towards the solution for current problems on regulation and activity of NMT2 which is responsible for the development of cancer.

Furthermore, the results in this study have demonstrated the increased proliferation rates in MCF7 cells due to nuclear NMT2 while the absence of it shows lower cell proliferation rate. Nuclear NMT2 plays a key role in transcription rates of the IGF1R gene and the IGF1R protein expression in MCF7 cells. We show in this study that increased nuclear NMT2 is directly proportional to the increased IGF1R protein expression and to increased cell proliferation rate. Since IGF1R is one of the transmembrane protein receptors responsible for initiating activity in the IGF pathway, it is plausible that the increased expression of IGF1R is leading to increased activity in the IGF pathway and increased growth and proliferation in ER+ MCF7 breast cancer

cells. The mathematical model of this mitogenic signaling pathway is the key focus in this study. It shows the expression pattern of proteins involved in the pathway in different treatments and in various conditions. Also, it opens the door for improvement and better prediction for other treatments which could be very hard to achieve experimentally.

Chapter 8

Future Directions

This study opens many doors towards the investigation and understanding of the mitogenic signaling pathway leading to NMT2 and phospho-NMT2 regulation inside ER+ breast cancer cells. I believe the designed mathematical model could be updated for better understanding of the pathway using the following conditions:

1. A mathematical model for rapamycin-treated ER+ breast cancer cells could help investigate the NMT2 and pNMT2 expression pattern when the pathway is completely blocked or partially blocked.

2. Introduction of time delays to the ordinary differential equations for explaining the dynamics of the cell pathway might be very complex but would be helpful getting close to better prediction of protein status and expression in real time.

3. The model could be used to study other cell lines as well as various cancer types other than breast cancer.

In the future direction apart from the models explained in chapter 3, a few other models were also designed with taking some more factors into consideration such as time delays during the transcription and translation processes in cell. Time delays reflects mainly the transmission time between two interconnected data points, the processing time or the time taken to act

upon some signal. The complexity of biological networks inference from time series data. The time delays are used in Delayed Differential Equations to explain the dynamics of biological models and here also, I have used to delayed differential equations. The parameters in which delays have been introduced are the function of time with delay τ instead of state variables.

Even though necessary biological experiments required for these models were not be completed due to factors such as not having abundance of time in this current scenario of pandemic, these models open doors to countless possibilities of biological experimentation to add value to the robustness of the model. The extended models are as follows:

8.1 Time Delay Models: Insulin Treatment

These models are the extension of *Model 1: Insulin Treatment* where time delays are introduced at certain points. We have introduced a two-delay model where there are two state variables as function of time which incorporate transcription and translation process in the mathematical model. Also, to go from two-delay model to one-delay model we have introduced new variables in the systems of differential equations.

8.1.1 Two Delay Model

In the above figure 8.1, τ_1 and τ_2 have been introduced in the model where τ_1 represents the time taken for transcription from pNMT2 to IGF1R and τ_2 represents the time taken for the process of translation from IGF1R(mRNA) to IGF1R protein in the cytoplasm. The system of delayed differential equations explaining these dynamics are as follows:

$$\frac{dI_1}{dt} = \overbrace{\pi_{I_{1r}} I_{1r}(t-\tau_2)}^{synthesis} + \overbrace{\frac{\alpha_{I_{1p}} I_{1p}}{K_{I_{1p}} + I_{1p}}}^{dephosphorylation} - \overbrace{\frac{\alpha_{I_1} I_1}{K_{I_1} + I_1}}^{phosphorylation} \tag{8.1a}$$

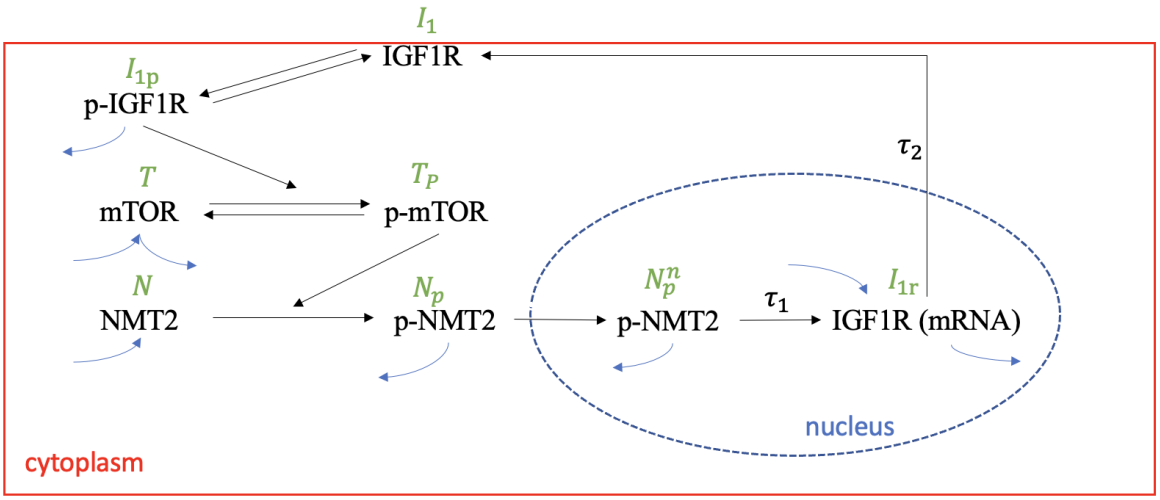

FIGURE 8.1: Two Delay Model: Insulin Treatment. In the flow diagram of the insulin treated model, two delays were inserted in the dynamics for the consideration of time taken by the transcription and translation.

$$\frac{dI_{1p}}{dt} = \overbrace{\frac{\alpha_{I_1} I_1 I_2}{K_{I_1} + I_1}}^{phosphorylation} - \overbrace{\frac{\alpha_{I_{1p}} I_{1p}}{K_{I_{1p}} + I_{1p}}}^{dephosphorylation} - \overbrace{\delta_{I_{1p}} I_{1p}}^{degradation} \tag{8.1b}$$

$$\frac{dT}{dt} = \overbrace{\Pi_T}^{baseline} + \overbrace{\frac{\alpha_{T_p} T_p}{K_{T_p} + T_p}}^{dephosphorylation} - \overbrace{\frac{\alpha_T I_{1p} T}{K_T + T}}^{phosphorylation} - \overbrace{\delta_T T}^{degradation} \tag{8.1c}$$

$$\frac{dT_p}{dt} = \overbrace{\frac{\alpha_T I_{1P} T}{K_T + T}}^{phosphorylation} - \overbrace{\frac{\alpha_{T_p} T_p}{K_{T_p} + T_p}}^{dephosphorylation} \tag{8.1d}$$

$$\frac{dN}{dt} = \overbrace{\Pi_N}^{baseline} - \overbrace{\frac{\alpha_N T_p N}{K_N + N}}^{phosphorylation} \tag{8.1e}$$

$$\frac{dN_p}{dt} = \overbrace{\frac{\alpha_N T_p N}{K_N + N}}^{phosphorylation} - \overbrace{\mu N_p}^{nucleus} - \overbrace{\delta_{N_p} N_p}^{degradation} \tag{8.1f}$$

$$\frac{dN_p^n}{dt} = \overbrace{\mu \left[\frac{V_c}{V_n}\right] N_p}^{nucleus} - \overbrace{\frac{\alpha_{N_p^n} N_p^n}{K_{N_p^n} + N_p^n}}^{complex\ formation} - \overbrace{\delta_{N_p^n} N_p^n}^{degradation} \tag{8.1g}$$

$$\frac{dI_{1r}}{dt} = \overbrace{\Pi_1}^{baseline} + \overbrace{\delta N_p^n(t-\tau_1)}^{DNAbinding} - \overbrace{\delta_{I_{1r}} I_{1r}}^{degradation} \tag{8.1h}$$

8.1.2 Single Delay Model

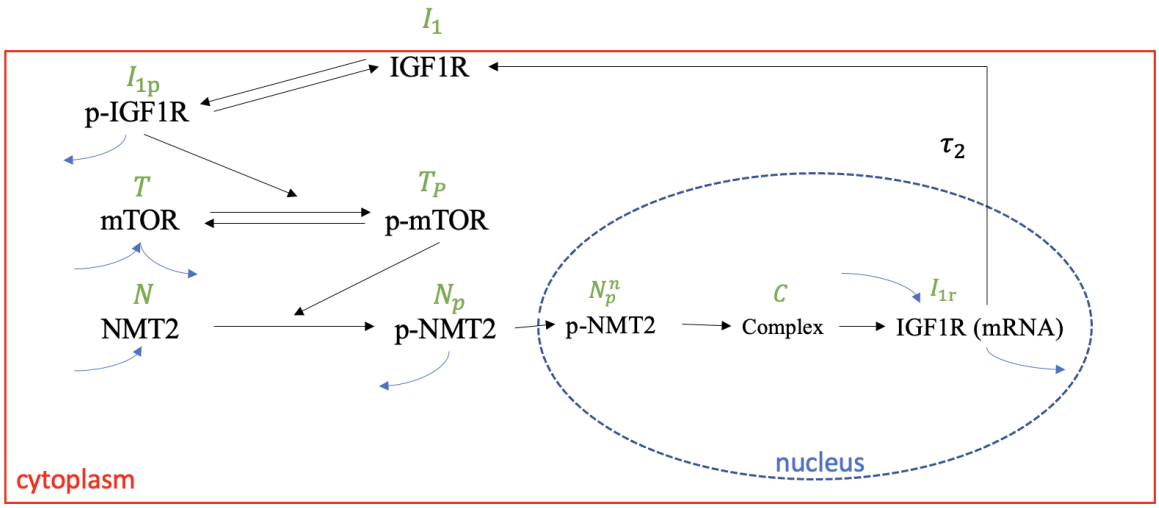

FIGURE 8.2: Single Delay Model: Insulin Treatment. To go to one delay from two delays, an additional variable (complex C) has been inserted replacing transcription delay τ_1.

Introducing delays in the differential equations makes the system complex and so, we tried to reduce the complexity of the model by reducing the time delays by introducing another variable into the system of equations i.e., C which represents the complex formed by the binding of pNMT2 to DNA acting as a transcription factor further to form IGF1R(mRNA). IGF1R(mRNA) after formation translocates out of the nucleus and then leads to exocytosis [33]. The set of differential equations explaining the dynamics in this system is as follows:

$$\frac{dI_1}{dt} = \overbrace{\pi_{I_{1r}} I_{1r}(t-\tau_2)}^{synthesis} + \overbrace{\frac{\alpha_{I_{1p}} I_{1p}}{K_{I_{1p}} + I_{1p}}}^{dephosphorylation} - \overbrace{\frac{\alpha_{I_1} I_1}{K_{I_1} + I_1}}^{phosphorylation} \tag{8.2a}$$

$$\frac{dI_{1p}}{dt} = \overbrace{\frac{\alpha_{I_1} I_1 I_2}{K_{I_1} + I_1}}^{phosphorylation} - \overbrace{\frac{\alpha_{I_{1p}} I_{1p}}{K_{I_{1p}} + I_{1p}}}^{dephosphorylation} - \overbrace{\delta_{I_{1p}} I_{1p}}^{degradation} \tag{8.2b}$$

$$\frac{dT}{dt} = \overbrace{\Pi_T}^{baseline} + \overbrace{\frac{\alpha_{T_p} T_p}{K_{T_p} + T_p}}^{dephosphorylation} - \overbrace{\frac{\alpha_T I_{1p} T}{K_T + T}}^{phosphorylation} - \overbrace{\delta_T T}^{degradation} \tag{8.2c}$$

$$\frac{dT_p}{dt} = \overbrace{\frac{\alpha_T I_{1P} T}{K_T + T}}^{phosphorylation} - \overbrace{\frac{\alpha_{T_p} T_p}{K_{T_p} + T_p}}^{dephosphorylation} \tag{8.2d}$$

$$\frac{dN}{dt} = \overbrace{\Pi_N}^{baseline} - \overbrace{\frac{\alpha_N T_p N}{K_N + N}}^{phosphorylation} \tag{8.2e}$$

$$\frac{dN_p}{dt} = \overbrace{\frac{\alpha_N T_p N}{K_N + N}}^{phosphorylation} - \overbrace{\mu N_p}^{nucleus} - \overbrace{\delta_{N_p} N_p}^{degradation} \tag{8.2f}$$

$$\frac{dN_p^n}{dt} = \overbrace{\mu \left[\frac{V_c}{V_n}\right] N_p}^{nucleus} - \overbrace{\frac{\alpha_{N_p^n} N_p^n}{K_{N_p^n} + N_p^n}}^{complex\ 1\ formation} - \overbrace{\delta_{N_p^n} N_p^n}^{degradation} \tag{8.2g}$$

$$\frac{dC}{dt} = \overbrace{\frac{\alpha_{N_p^n} N_p^n}{K_{N_p^n} + N_p^n}}^{complex\ 1\ formation} - \overbrace{\frac{\alpha_C C}{K_C + C}}^{RNA\ formation} \tag{8.2h}$$

$$\frac{dI_{1r}}{dt} = \overbrace{\Pi_1}^{baseline} + \overbrace{\frac{\alpha_C C}{K_C + C}}^{RNAformation} - \overbrace{\delta_{I_{1r}} I_{1r}}^{degradation} \tag{8.2i}$$

8.2 Time Delay Models: Control

8.2.1 Two Delay Model: Control

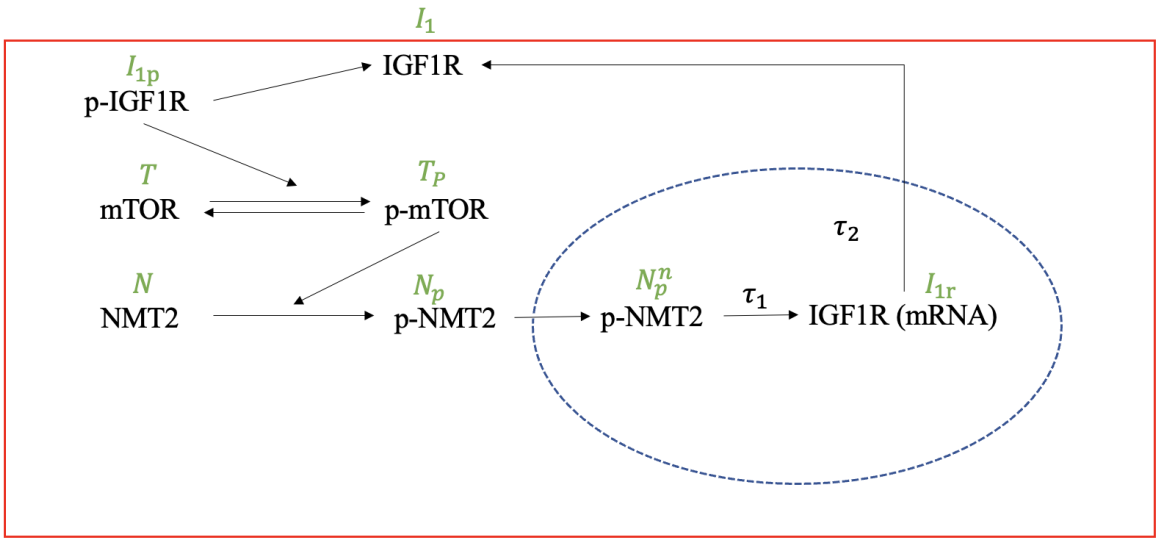

FIGURE 8.3: Two-Delay Model: Control. In the flow diagram of the control model, two delays were inserted in the dynamics for the consideration of time taken by the transcription and translation.

The above figure 8.3 represents the flow diagram of the pathway in the two-delay model system where the Complex C has been introduced in the two delay model system to reduce the complexity due to delays. The set of differential equations explaining this dynamics is as follows:

$$\frac{dI_1}{dt} = \overbrace{\pi_{I_{1r}} I_{1r}(t-\tau_2)}^{synthesis} + \overbrace{\frac{\alpha_{I_{1p}} I_{1p}}{K_{I_{1p}} + I_{1p}}}^{dephosphorylation} \tag{8.3a}$$

$$\frac{dI_{1p}}{dt} = -\overbrace{\frac{\alpha_{I_{1p}} I_{1p}}{K_{I_{1p}} + I_{1p}}}^{dephosphorylation} - \overbrace{\delta_{I_{1p}} I_{1p}}^{degradation} \tag{8.3b}$$

$$\frac{dT}{dt} = \overbrace{\Pi_T}^{baseline} + \overbrace{\frac{\alpha_{T_p} T_p}{K_{T_p} + T_p}}^{dephosphorylation} - \overbrace{\frac{\alpha_T I_{1p} T}{K_T + T}}^{phosphorylation} - \overbrace{\delta_T T}^{degradation} \tag{8.3c}$$

$$\frac{dT_p}{dt} = \overbrace{\frac{\alpha_T I_{1P} T}{K_T + T}}^{phosphorylation} - \overbrace{\frac{\alpha_{T_p} T_p}{K_{T_p} + T_p}}^{dephosphorylation} \tag{8.3d}$$

$$\frac{dN}{dt} = \overbrace{\Pi_N}^{baseline} - \overbrace{\frac{\alpha_N T_p N}{K_N + N}}^{phosphorylation} \tag{8.3e}$$

$$\frac{dN_p}{dt} = \overbrace{\frac{\alpha_N T_p N}{K_N + N}}^{phosphorylation} - \overbrace{\mu N_p}^{nucleus} - \overbrace{\delta_{N_p} N_p}^{degradation} \tag{8.3f}$$

$$\frac{dN_p^n}{dt} = \overbrace{\mu \left[\frac{V_c}{V_n}\right] N_p}^{nucleus} - \overbrace{\frac{\alpha_{N_p^n} N_p^n}{K_{N_p^n} + N_p^n}}^{Complex\ formation} - \overbrace{\delta_{N_p^n} N_p^n}^{degradation} \tag{8.3g}$$

$$\frac{dI_{1r}}{dt} = \overbrace{\Pi_1}^{baseline} + \overbrace{\delta N_p^n (t - \tau_1)}^{DNAbinding} - \overbrace{\delta_{I_{1r}} I_{1r}}^{degradation} \tag{8.3h}$$

8.2.2 Single Delay Model: Control

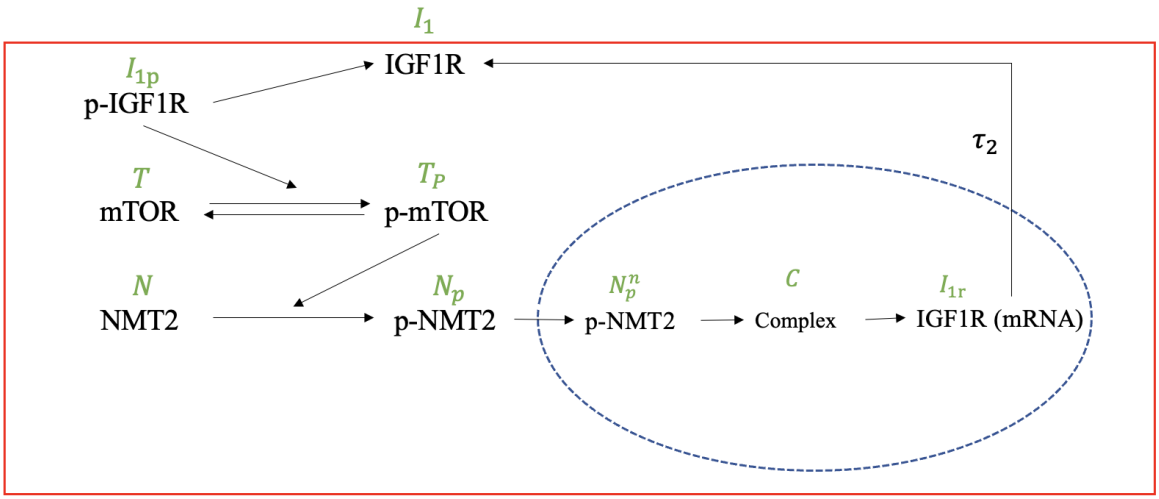

FIGURE 8.4: Single Delay Model: Control. To go to one delay from two delays, an additional variable (complex C) has been inserted replacing transcription delay τ_1.

Figure 8.4 represents the flow diagram of the pathway in One-delay model without any treatments. In this system, the complex formed by binding of NMT2 to DNA has been considered as a variable to reduce the number of delays in order to simplify the complexity of the model. The set of differential equations for this system are as follows:

$$\frac{dI_1}{dt} = \overbrace{\pi_{I_{1r}} I_{1r}(t-\tau_2)}^{synthesis} + \overbrace{\frac{\alpha_{I_{1p}} I_{1p}}{K_{I_{1p}} + I_{1p}}}^{dephosphorylation} \tag{8.4a}$$

$$\frac{dI_{1p}}{dt} = -\overbrace{\frac{\alpha_{I_{1p}} I_{1p}}{K_{I_{1p}} + I_{1p}}}^{dephosphorylation} - \overbrace{\delta_{I_{1p}} I_{1p}}^{degradation} \tag{8.4b}$$

$$\frac{dT}{dt} = \overbrace{\Pi_T}^{baseline} + \overbrace{\frac{\alpha_{T_p} T_p}{K_{T_p} + T_p}}^{dephosphorylation} - \overbrace{\frac{\alpha_T I_{1p} T}{K_T + T}}^{phosphorylation} - \overbrace{\delta_T T}^{degradation} \tag{8.4c}$$

$$\frac{dT_p}{dt} = \overbrace{\frac{\alpha_T I_{1P} T}{K_T + T}}^{phosphorylation} - \overbrace{\frac{\alpha_{T_p} T_p}{K_{T_p} + T_p}}^{dephosphorylation} \tag{8.4d}$$

$$\frac{dN}{dt} = \overbrace{\Pi_N}^{baseline} - \overbrace{\frac{\alpha_N T_p N}{K_N + N}}^{phosphorylation} \tag{8.4e}$$

$$\frac{dN_p}{dt} = \overbrace{\frac{\alpha_N T_p N}{K_N + N}}^{phosphorylation} - \overbrace{\mu N_p}^{nucleus} - \overbrace{\delta_{N_p} N_p}^{degradation} \tag{8.4f}$$

$$\frac{dN_p^n}{dt} = \overbrace{\mu \left[\frac{V_c}{V_n}\right] N_p}^{nucleus} - \overbrace{\frac{\alpha_{N_p^n} N_p^n}{K_{N_p^n} + N_p^n}}^{Complex\ formation} - \overbrace{\delta_{N_p^n} N_p^n}^{degradation} \tag{8.4g}$$

$$\frac{dC}{dt} = \overbrace{\frac{\alpha_{N_p^n} N_p^n}{K_{N_p^n} + N_p^n}}^{Complex\ formation} - \overbrace{\frac{\alpha_C C}{K_C + C}}^{RNA\ formation} \tag{8.4h}$$

$$\frac{dI_{1r}}{dt} = \overbrace{\Pi_1}^{baseline} + \overbrace{\frac{\alpha_C C}{K_C + C}}^{RNA formation} - \overbrace{\delta_{I_{1r}} I_{1r}}^{degradation} \tag{8.4i}$$

Appendix A

Reagents Preparation

A.1 Incomplete (without antibiotics) DMEM-1L

- Dulbecco's modified eagle medium powder-1 packet
- 1 litre of double distilled water
- 3.7g of Na_2CO_3
- Adjust pH to 7.2 using HCl or NaOH
- Filter using 0.22μ filter
- Storage: 4^o C

A.2 10% Supplemented DMEM-1L

- 900ml incomplete DMEM
- 100ml Fetile Bovine Serum (FBS)
- 10 ml streptomycin penicillin solution
- 10ml of 30% glucose
- 10ml of L-glutamine

A.3 10X PBS-1000mL (pH 6.8)

- 17.8g $Na_2HPO_4.2H_2O$
- 2.4g KH_2PO_4
- 80g NaCl
- 2g Kcl
- 1L distilled H_2O

A.4 Complete Lysis Buffer-500ml

- 5.975g Hepes (pH 7.4, 50 mM)
- 25.67g sucrose (150 mM)
- 5mL 200mM sodium orthovandate (2mM) 12.24g glycerolphosphate (80mM)
- 0.21g sodium floride (10mM)
- 2.23g sodium phosphate (10mM)
- 2mL 0.5M EGTA (2mM)
- 2mL 0.5M EDTA (2mM)
- 5mL Trixton X-100 (1%)
- 0.5g SDS (0.1%)
- 20μl 1mM PMSF (100mM)
- 20 μL protease cocktail inhibitor (1%)

A.5 4X Bromophenol Blue Sample Loading buffer

- 2.422g 200 mM Tris (pH 6.8)
- 0.4% bromophenol blue
- 4mL glycerol
- 8% SDS (should be added last)
- Fill upto 10mL with distilled H_2O
- add dithiothreitol (DTT) to the ratio of 9:1 with the mixture

A.6 5% Stacking Gel

- 2.1mL distilled water
- 0.5mL 30% acrylamide
- 0.38mL Tris-Cl (1.0M, pH 6.8)
- 0.03mL 10% SDS
- 0.03mL 10% ammonium persulphate (APS)
- 3μl Tetramethylethylenediamine (TEMED)

A.7 10% Resolving Gel

- 4.0mL distilled H_2O
- 3.3mL 30% acrylamide
- 2.5mL Tris-Cl (1.5M, pH 8.8)
- 0.1mL 10% SDS

- 0.1mL 10% ammonium persulphate (APS)
- 4μL Tetramethylethylenediamine (TEMED)

A.8 Resolving Gel for PhosTag SDS-PAGE-10mL

- 4mL 30% Acrylamide Solution
- 2.5mL 1.4M Bis-Tris/HCl Solution
- 0.1mL 5mM Phos-tag AAL Solution
- 10μl 10mM $ZnCl_2$ Solution
- 3.24mL double distilled water
- 10μl TEMED(tetramethylenediamine)
- 50μl 10% APS(ammonium peroxydisulphate)

A.9 Stacking Gel for PhosTag SDS-PAGE

- 1.5mL 30% Acrylamide Solution
- 2.5mL 1.4M Bis-Tris/HCl Solution
- 5.94mL double distilled water
- 10μl TEMED
- 50μl APS

A.10 Freezing Media-50mL

- 45mL FBS
- 5mL DMSO

A.11 30% acrylamide solution-200mL

- 58.0g acrylamide
- 2.0g N,N′-methylene-bisacrylamide
- 200mL double distilled water

A.12 5mM Phos-Tag AAL Solution containing 3% MeOH

- 10mg Phos-tag AAL-107
- 0.10 mL methanol
- 3.2mL double distilled water

A.13 0.5M Sodium Bisulfite

- 5.3g $NaHSO_3$
- 100mL double distilled water

A.14 1.4M Bis-Tris/HCl Solution, pH-6.8

- 29.9g Bis-Tris base (MW: 209)
- 10mL of 6M HCl
- 100mL double distilled water

A.15 Mild Stripping Buffer-1L, pH-2.2

- 800ml distilled water
- 15g glycine
- 1g SDS
- 10ml Tween-20
- Bring Volume up to 1L with distilled water

A.16 Harsh Stripping Buffer-100ml

- 67.5ml distilled water
- 20ml SDS
- 12.5 ml of 0.5M Tris-HCl, pH-6.8
- 0.8ml β-mercaptoethanol

Appendix B

Supplementary Data

B.1 Quantification of IGF1R protein expression

Treatment	0.5h	1h	6h	24h
Control	0.025	0.048	0.099	0.083
Insulin	0.035	0.079	0.193	0.333
Rapamycin	0.075	0.089	0.112	0.083
DMSO	0.05	0.092	0.205	0.081

TABLE B.1: Normalized quantification of the IGF1R protein expression in Control, Insulin treated, Rapamycin treated, and DMSO treated MCF7 cell lysates for 30 minutes, 60 minutes, 360 minutes, and 1440 minutes. The normalization of IGF1R protein was done against the β-actin expression value.

B.2 Quantification of protein expression from the Western Blot Analysis

B.2.1 Control

Control	0.5h	1h
Nuclear pNMT2	157,015.93	1,010,971.26
Nuclear NMT2	558,690.76	369,371.82
Cytoplasmic pNMT2	48,446.51	-114,017.88
Cytoplasmic NMT2	1,084,925.41	2,745,038.25
Total	1,849,078.61	4,011,363.45
Nuclear pNMT2/Total	0.084915766	0.252026842
Nuclear pNMT2/Nuclear NMT2	0.281042643	2.737001633
Control	**6h**	**24h**
Nuclear pNMT2	2,843,126.88	2,646,315.06
Nuclear NMT2	420,937.00	1,786,708.00
Cytoplasmic pNMT2	-147,170.50	98,597.80
Cytoplasmic NMT2	1,482,423.00	1,202,214.14
Total	4,599,316.38	5,733,835.00
Nuclear pNMT2/Total	0.618162928	0.461526196
Nuclear pNMT2/Nuclear NMT2	6.754281223	6.643392362

TABLE B.2: Normalized quantitative expression of Nuclear NMT2, Nuclear phospho NMT2, Cytoplasmic NMT2, and Cytoplasmic phospho NMT2 for control MCF7 cells. The relative expression pattern of pNMT2 protein for the indicated time points was generated by taking the ratio of pNMT2 expression to Nuclear NMT2 in the figure B.1 and the ratio of pNMT2 expression to Total in the figure B.2

B.2.2 Insulin

Insulin	**0.5h**	**1h**
Nuclear pNMT2	327,300.63	1,299,147.63
Nuclear NMT2	592,686.59	539,067.78
Cytoplasmic pNMT2	-45,218.85	-4,797.68
Cytoplasmic NMT2	842,491.15	3,353,894.54
Total	1,717,259.51	5,187,312.26
Nuclear pNMT2/Total	0.190594742	0.250447161
Nuclear pNMT2/Nuclear NMT2	0.552232229	2.409989409
Insulin	**6h**	**24h**
Nuclear pNMT2	3,133,948.88	3,067,872.80
Nuclear NMT2	373,766.00	1,826,229.00
Cytoplasmic pNMT2	-201,088.50	45,448.51
Cytoplasmic NMT2	1,406,383.00	946,477.77
Total	4,713,009.38	5,886,028.09
Nuclear pNMT2/Total	0.664957064	0.521212736
Nuclear pNMT2/Nuclear NMT2	8.384788544	7.997717525

TABLE B.3: Normalized quantitative expression of Nuclear NMT2, Nuclear phospho NMT2, Cytoplasmic NMT2, and Cytoplasmic phospho NMT2 for insulin treated MCF7 cells. The relative expression pattern of pNMT2 protein for the indicated time points was generated by taking the ratio of pNMT2 expression to Nuclear NMT2 in the figure B.1 and the ratio of pNMT2 expression to Total in the figure B.2

B.3 Relative nuclear pNMT2 expression in MCF7 Cells: Control, Insulin, and Rapamycin treatment

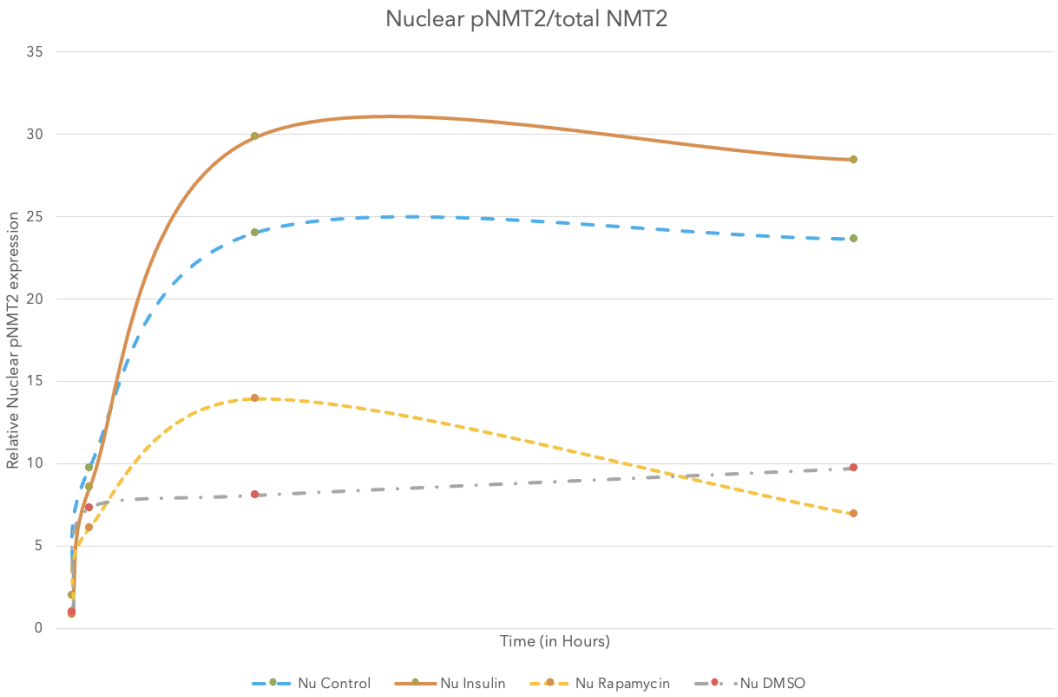

FIGURE B.1: Relative Nuclear pNMT2 expression for Control,Insulin, and Rapamycin treated MCF7 cells with DMSO as a control for rapamycin. The fold increase/decrease values were calculated by fixing the Control 0.5h and DMSO 0.5h as 1 for comparison with insulin and rapamycin treatment respectively

B.4 Relative nuclear pNMT2 expression in MCF7 Cells: Control and Insulin treatment

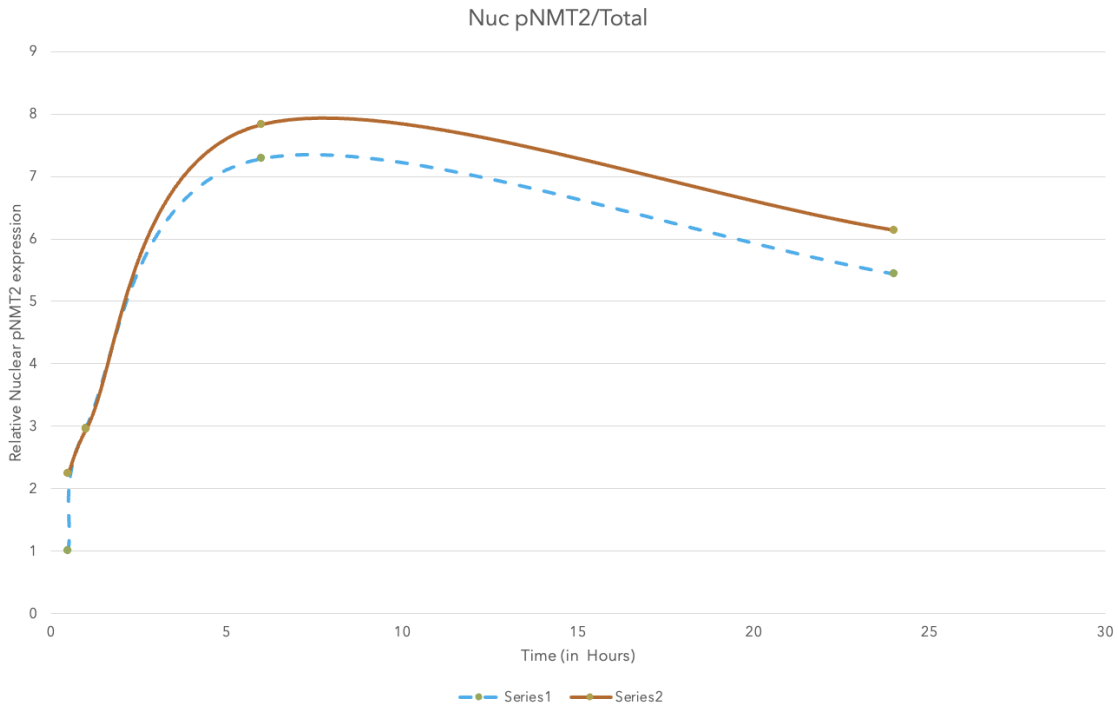

FIGURE B.2: Relative Nuclear pNMT2 expression for Control, and Insulin treated MCF7 cells with DMSO as a control for rapamycin. The fold increase/decrease values were calculated by fixing the Control 0.5h. The relative expression of nuclear pNMT2 were calculated by taking ratio of Nuclear pNMT2 and Total expression mentioned in the table 3.1

B.5 Crystal Violet Cell Proliferation Assay

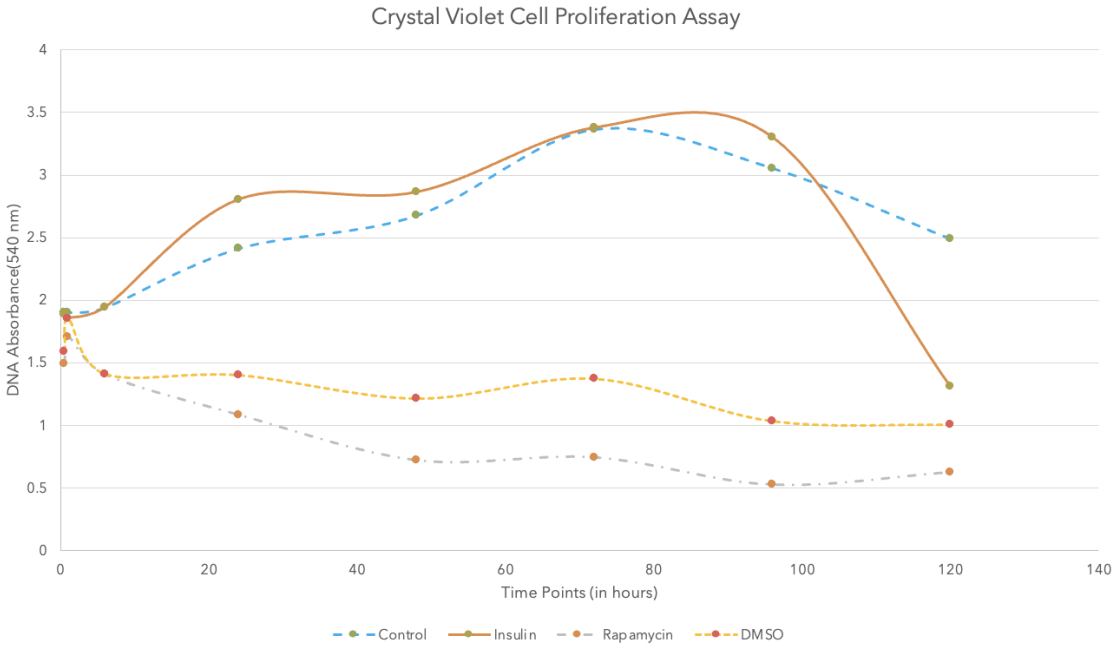

FIGURE B.3: Crystal Violet assay of cellular proliferation rate of control, insulin treated, rapamycin treated, and DMSO treated MCF7 cells. Each point is an average of six biological replicates. We see decrease in the proliferation rate for control and insulin treated MCF7 cells after 72h and 90h respectively due to lack of space for cells to grow. Once the cells reach complete confluency, they tend to kill the other cells. Another reason for the decrease in the rate is the decrease in available nutrients for the cells to grow. Available nutrients starts to decrease in a faster rate with increase in number of cells.

B.6 Co-ImmunoPrecipitation

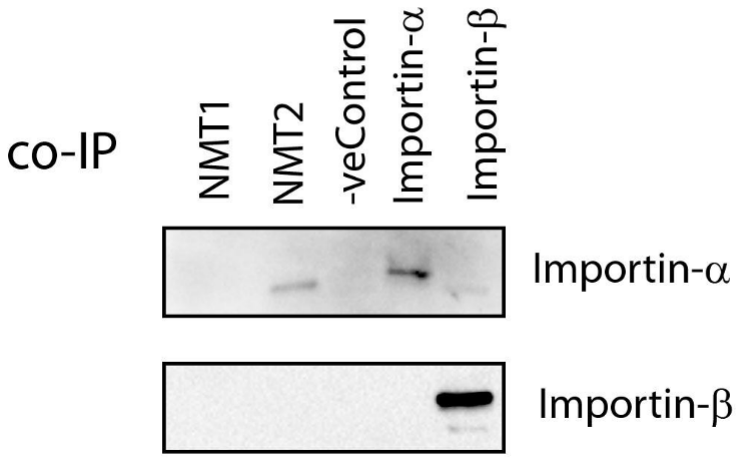

FIGURE B.4: Western blot image of importin-α mediated NMT2 nuclear translocation. Presence of NMT2 and importin-α expression suggests the protein-protein interaction between the proteins whereas there is no such protein protein interactions between NMT1 and importin-α or NMT2 and importin-β. Rabbit IgG and Mouse IgG were used as negative control for antibodies developed in rabbit and mouse respectively

B.7 Protein expression in insulin treated and IGF1 treated MCF7 cells

B.7.1 NMT2 (monoclonal)

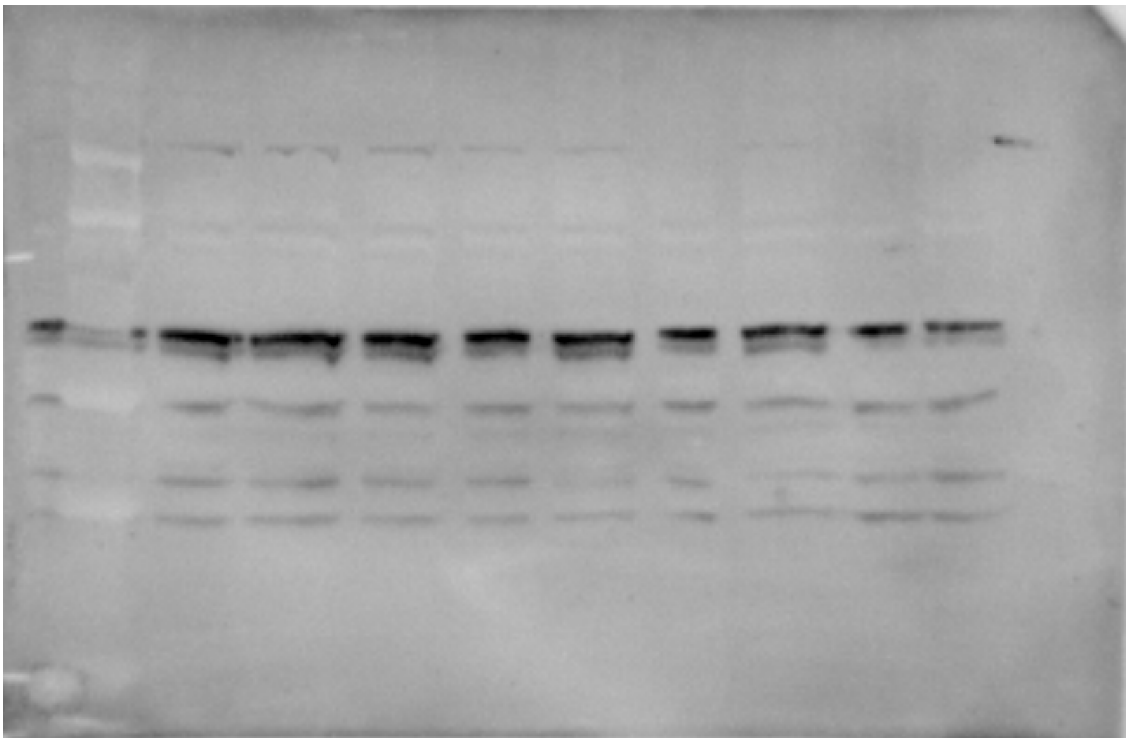

FIGURE B.5: NMT2 protein expression in MCF7 cell lysates treated with insulin and IGF1 for 30 minutes, 60 minutes, 360 minutes, and 1440 minutes. Left to right: Ins 24h, Ins 6h, Ins 1h, Ins 0.5h, Control, IGF1 0.5h, IGF1 1h, IGF1 6h, IGF1 24h.

B.7.2 phospho AKT

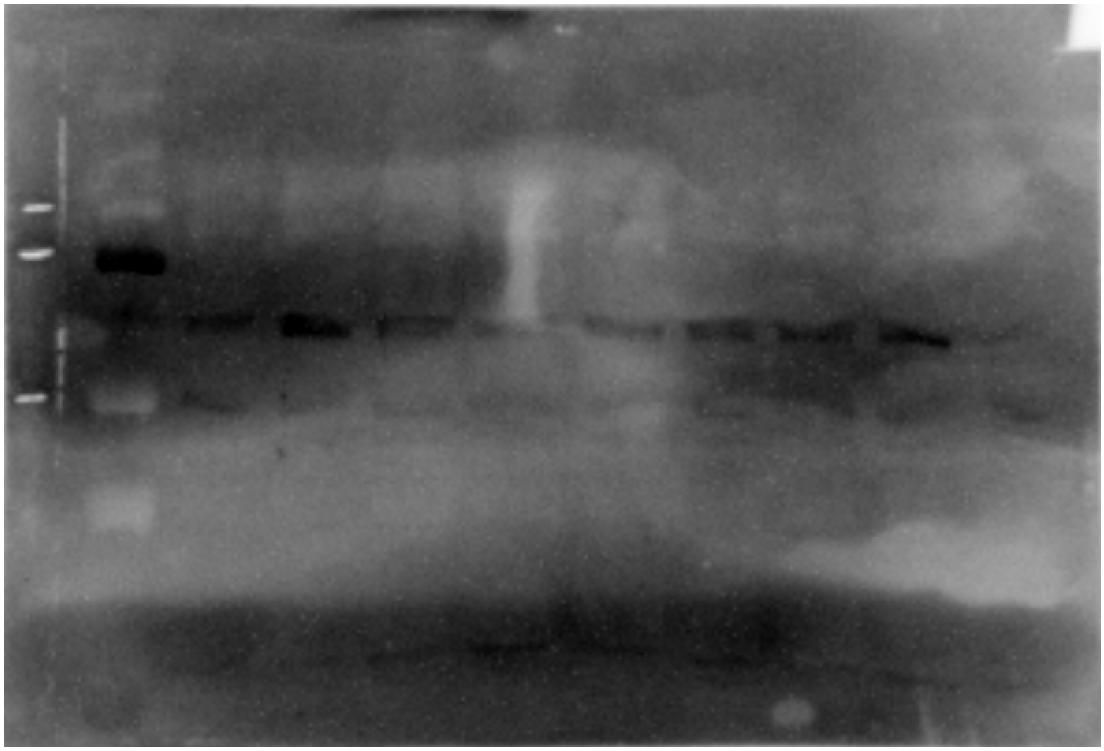

FIGURE B.6: Phospho AKT protein expression in MCF7 cell lysates treated with insulin and IGF1 for 30 minutes, 60 minutes, 360 minutes, and 1440 minutes. Left to right: Ins 24h, Ins 6h, Ins 1h, Ins 0.5h, Control, IGF1 0.5h, IGF1 1h, IGF1 6h, IGF1 24h.

B.7.3 phospho mTOR

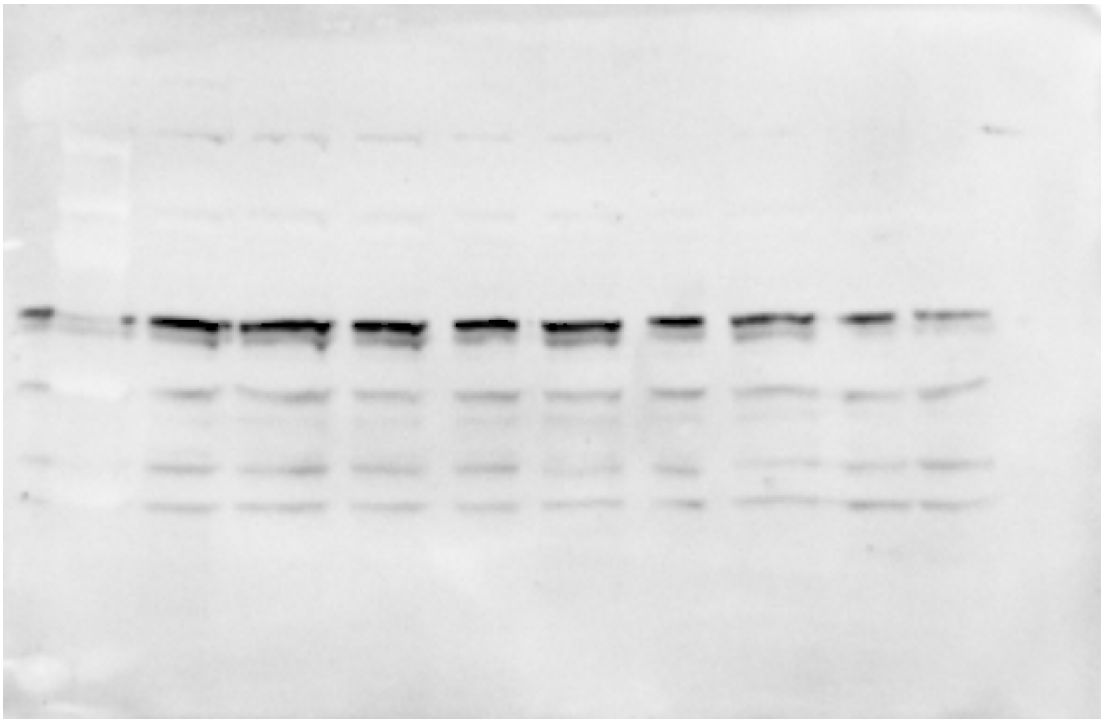

FIGURE B.7: Phospho mTOR protein expression in MCF7 cell lysates treated with insulin and IGF1 for 30 minutes, 60 minutes, 360 minutes, and 1440 minutes. Left to right: Ins 24h, Ins 6h, Ins 1h, Ins 0.5h, Control, IGF1 0.5h, IGF1 1h, IGF1 6h, IGF1 24h.

B.8 RNA isolation

WT MCF7 cells with approximately 90% confluency (around 1.5×10^6 cells) treated with 100nM insulin, 100nM rapamycin, and DMSO for 0.5h, 1h, 6h and 24h. RNA was extracted using E.Z.N.A. Total RNA Kit I, (Omega biotek) as per manufacturer recommendations. For each respective timepoints, the media was then siphoned off from the T25 flasks and the cells were lysed with 350ml TRK lysis buffer with 2% β-mercaptoethanol in it. The mixture was collected in a microcentrifuge tube and then homogenized using syringe and needle (19-21 gauge) for 5-10 times to shear high molecular weight DNA. Equal volume of 70% ethanol was added to it following vortexing to mix it

TABLE B.4: RNA quantification and cDNA synthesis calculation

Sample	**RNA conc. (ng/μL)**	**1μg RNA (μL)**	**Nuclease free water (μL)**
Control 0.5h	89.3	11.20	1.80
Control 1.0h	308.7	3.24	9.76
Control 6.0h	361	2.77	10.23
Control 24h	371.9	2.7	10.3
Insulin 0.5h	663.3	1.51	11.49
Insulin 1.0h	436	2.29	10.71
Insulin 6.0h	864.1	1.16	11.84
Insulin 24h	85.5	11.70	1.3

thoroughly. The mixture was transferred to a HiBind RNA Mini Column set on a 2 mL collection tube. The tube was then centrifuged at 10000 $\times$ g for 1 minute. The filtrate was discarded, and the previous step was repeated 7-10 times reusing the same collection tube until all the sample has been transferred to the column. Then 500ml of RNA wash buffer I was added to the mini column and centrifuged at 10000xg for 30 seconds. Filtrate was discarded and 500ml RNA wash buffer II was added to it and centrifuged it for 1 minute twice. Then centrifugation was done again at the maximum speed for 2 minutes. The Mini Column was transferred to a clean 1.5mL microcentrifuge tube and 40ml Nuclease DEPC water (70°C) was added and centrifuged for 2 minutes at maximum speed. The previous step was repeated without discarding the filtrate. RNA concentration quantification was done (see Table B.4), and the elution was stored at -70°C for further purpose.

B.9 cDNA Synthesis

The extracted RNA was used to generate cDNA using iScript cDNA synthesis Kit (Bio-Rad) as per manufacturer's instructions. Mastermix was prepared using 4μL,1 μL and 2μL of 5x iScript select reaction mix, iScript reverse transcriptase and random primers respectively per reaction. The components

mentioned in table B.4 were thawed on ice and mixed according to the calculation in a 0.2 mL PCR tube. Those were incubated for 5 mins at 25°C and then incubated for 5 min at 85°C to heat activate the reverse transcriptase. The cDNA product was stored at 4°C and used later for PCR amplification.

B.10 qPCR

IGF1R gene expression was analyzed using quantitative Polymerase Chain Reaction (qPCR). The reactions were set up in hard shell 96 PCR well plates (Bio-Rad) and performed using SsoAdvanced Universal SYBR Green Supermix reagent (Bio-Rad) according to the manufacturers protocol. Each reaction well has a final volume of 20μL and consists of 10μL of SSoAdvanced universal SYBR Green supermix (2X), 500nm of forward primers and 500nm of reverse primers and 100ng of cDNA.

IGF1R forward and reverse primers were obtained from Thermo Fisher. Housekeeping control genes included GAPDH (Invitrogen) and RPLOP (Invitrogen). All IGF1R, GAPDH, and RPLOP reactions were run in triplicate along with no template control (NTC) wells. A CFX connected Real-Time thermocycler (Bio-Rad) was used to perform the PCR. The setting is as follows: 1 cycle of 95°C for 30 seconds (Polymerase activation), 35 cycles of 95°C for 10 seconds (DNA denaturation), 60°C for 30 seconds (annealing, extension and plate read), 65°C to 95°C for 5 seconds (melt curve analysis). An IGF1R gene expression bar graph was compiled by CFX Manager 3.1 software. The graph was produced using the MCF7 WT cell line as the reference IGF1R gene expression line.

Bibliography

[1] BreastCancer.Org. "Molecular Subtypes of Breast Cancer". In: (Mar. 2019). URL: https://www.breastcancer.org/symptoms/types/molecular-subtypes.

[2] Govt. of Canada. "Breast Cancer". In: (2019). URL: https://www.canada.ca/en/public-health/services/chronic-diseases/cancer/breast-cancer.html.

[3] A Anderson *et al*. "Microenvironmental Independence Associated with Tumor Progression". In: American Association of Cancer Research (Nov. 2009). URL: https://doi.org/10.1158/0008-5472.CAN-09-0437.

[4] A Goldhirsch *et al*. " Personalizing the treatment of women with early breast cancer: highlights of the St Gallen International Expert Consensus on the Primary Therapy of Early Breast Cancer 2013 ". In: ANNALs of Oncology (Sept. 2013). URL: https://www.annalsofoncology.org/article/S0923-7534(19)36964-9/fulltext.

[5] A Shrivastav *et al*. "Expression of N-myristoyltransferase in Human Brain Tumors". In: Neurochemical Research (2005). URL: https://link.springer.com/article/10.1007/s11064-004-9680-9.

[6] A Shrivastav *et al*. "N-myristoyltransferase: A potential novel diagnostic masker for colon cancer". In: Journal of Translational Medicine (Nov. 2007). URL: https://translational-medicine.biomedcentral.com/articles/10.1186/1479-5876-5-58.

[7] B Will *et al*. "Estimates of the lifetime costs of breast cancer treatment in Canada". In: Europian Journal of Cancer (Apr. 2000). URL: https://pubmed.ncbi.nlm.nih.gov/10762744/.

[8] C K Osborne *et al*. "Human epidermal growth factor receptor-2-positive breast cancer: current management of early, advanced, and recurrent disease". In: Current Opinion in Obstetrics and Gynecology (Feb. 2011). URL: https://journals.lww.com/co-obgyn/Abstract/2011/02000/Human_epidermal_growth_factor_receptor_2_positive.9.aspx.

[9] C Oliveira *et al*. "Trends in use and cost of initial cancer treatment in Ontario: a population-based descriptive study". In: CMAJ Open (Dec. 2013). URL: https://pubmed.ncbi.nlm.nih.gov/25077117/.

[10] C Osborne *et al*. "MECHANISMS OF ENDOCRINE RESISTANCE IN BREAST CANCER". In: Annual Review of Medicine (Sept. 2010). URL: https://www.annualreviews.org/doi/abs/10.1146/annurev-med-070909-182917.

[11] C Thomas *et al*. "The different roles of ER subtypes in cancer biology and therapy". In: Nature Reviews Cancer (July 2011). URL: https://www.nature.com/articles/nrc3093.

[12] CB Matsen *et al*. "Breast cancer: a review for the general surgeon". In: JAMA Surgery (Oct. 2013). URL: https://jamanetwork.com/journals/jamasurgery/article-abstract/1732045.

[13] D Lamming *et al*. "Inhibition of the Mechanistic Target of Rapamycin". In: Cold Spring Harbour Perspectives in Medicine (2016). URL: http://perspectivesinmedicine.cshlp.org/content/6/5/a025924.

[14] D Xiaofeng *et al*. "Breast Cancer Cell Line Classification and Its Relevance with Breast Tumor Subtyping". In: Journal of Cancer (2017). URL: https://www.jcancer.org/v08p3131.htm.

[15] E. C. Inwald *et al*. "Ki-67 is a prognostic parameter in breast cancer patients: results..." In: Breast Cancer Research and Treatment (June 2013). URL: https://www.ncbi.nlm.nih.gov/pmc/articles/PMC3669503/.

[16] E Thenon *et al*. "N-Myristoyltransferase Inhibition Induces ER-Stress, Cell Cycle Arrest, and Apoptosis in Cancer Cells". In: ACS Chemical Biology (June 2016). URL: https://pubs.acs.org/doi/10.1021/acschembio.6b00371.

[17] G Arpino *et al*. "Crosstalk between the Estrogen Receptor and the HER Tyrosine Kinase Receptor Family". In: Endocrine Society (Apr. 2008). URL: https://academic.oup.com/edrv/article/29/2/217/2355051.

[18] H. Kanaizumi *et al*. "PI3K/Akt/mTOR signalling pathway activation in patients with ERpositive, metachronous, contralateral breast cancer treated with hormone therapy". In: Oncology Letter (Apr. 2002). URL: https://www.spandidos-publications.com/10.3892/ol.2018.9759.

[19] H Soule *et al*. "A Human Cell Line From a Pleural Effusion Derived From a Breast Carcinoma". In: Journal of the National Cancer Institute (Nov. 1973). URL: https://academic.oup.com/jnci/article/51/5/1409/962551.

[20] J Iwasa *et al*. "Karp's Cell and Molecular Biology: Concepts and Experiments". In: Karps cell and Molecular Biology (Dec. 2015). URL: https://www.wiley.com/en-ca/Karp%5C%27s+Cell+and+Molecular+Biology%5C%3A+Concepts+and+Experiments%5C%2C+8th+Edition-p-9781118886144.

[21] J Schnell *et al*. "Non-traditional functions of Ubiquitin and Ubiquitin-binding Proteins". In: Journal of Chemical Biology (Sept. 2003). URL: https://www.sciencedirect.com/science/article/pii/S0021925820833857.

[22] K Dietz *et al*. "Daniel Bernoulli's epidemiological model revisited". In: Mathematical Bioscience (Mar. 2002). URL: http://www.medicine.mcgill.ca/epidemiology/hanley/bios601/competingRisks/DanielBernoulli.pdf.

[23] K Kerlikowske *et al*. "Comparative effectiveness of digital versus film-screen mammography in community practice in the United States: a cohort study". In: Breast Cancer Surveillance Consortium (2011). URL: https://www.ncbi.nlm.nih.gov/pmc/articles/PMC3726800.

[24] L Ballou *et al*. " Rapamycin and mTOR kinase inhibitors ". In: Journal of Chemical Biology (May 2008). URL: https://link.springer.com/article/10.1007/s12154-008-0003-5.

[25] L Johnson *et al*. "The effects of Phosphorylation on the Structure and Functions of proteins". In: Annual Review of Biophysics (1993). URL: https://www.annualreviews.org/doi/10.1146/annurev.bb.22.060193.001215.

[26] M Bryant *et al*. "Myristoylation-dependent replication and assembly of human immunodeficiency virus 1". In: PNAS (Jan. 1990). URL: https://www.pnas.org/content/87/2/523.short.

[27] M Francipane *et al*. "mTOR pathway in colorectal cancer: an update". In: Oncotarget (Dec. 2013). URL: https://www.ncbi.nlm.nih.gov/pmc/articles/PMC3960188/.

[28] M Van Goethem *et al*. "Magnetic resonance imaging in breast cancer". In: Eur J Surg Oncol (2006). URL: https://pubmed.ncbi.nlm.nih.gov/16920327/.

[29] M Zhang *et al*. "Estrogen receptor-positive breast cancer molecular signatures and therapeutic potentials". In: Biomed Rep (Jan. 2014). URL: https://www.ncbi.nlm.nih.gov/pmc/articles/PMC3916982/.

[30] MC Gutierrez *et al*. "Molecular changes in Tamoxifen-Resistance Breast Cancer: Relationship between Estrogen Receptor, HER-2, and p38 Mitogen -Activated Protein Kinase". In: Journal of Clinical Oncology (Apr. 2008). URL: https://academic.oup.com/edrv/article/29/2/217/2355051.

[31] MH Wright *et al*. "Protein myristoylation in health and disease". In: Journal of Chemical Biology (2010). URL: https://www.ncbi.nlm.nih.gov/pmc/articles/PMC2816741/.

[32] P Bowyer *et al*. "N-Myristoyltransferase: a Prospective Drug Target for Protozoan Parasites". In: ChemMedChem (Mar. 2008). URL: https://chemistry-europe.onlinelibrary.wiley.com/doi/full/10.1002/cmdc.200700301.

[33] P Cao *et al*. "Activity-Dependent IGF-1 Exocytosis Is Controlled by the Ca2+-Sensor Synaptotagmin-10". In: Cell (Apr. 2011). URL: https://www.ncbi.nlm.nih.gov/pmc/articles/PMC3102833/.

[34] P Garcia *et al*. "Applied mathematics and nonlinear sciences in the war on cancer". In: Applied Mathematics and Non-linear Sciences (Sept. 2016). URL: https://www.sciendo.com/article/10.21042/AMNS.2016.2.00036.

[35] P Selvakumar *et al*. "Potential role of N-myristoyltransferase in cancer". In: Progress in lipid research (Jan. 2007). URL: https://pubmed.ncbi.nlm.nih.gov/16846646/.

[36] P Vlastaridis *et al*. "Estimating the total number of phosphoproteins and phophorylation sites in eukaryotic proteomes". In: GigaScience (Jan. 2017). URL: https://www.ncbi.nlm.nih.gov/pmc/articles/PMC5466708/.

[37] R Brady *et al*. "Mathematical Models of Cancer: When to Predict Novel Therapies, and When Not to". In: Bulletin of Mathematical Biology (July 2019). URL: https://link.springer.com/article/10.1007/s11538-019-00640-x.

[38] R Callahan *et al*. "Human epidermal growth factor receptor-2-positive breast cancer: Current management of early, advanced, and recurrent disease". In: Current Opinion in Obstetricks and gynecology (Feb. 2011). URL: https://journals.lww.com/co-obgyn/Abstract/2011/02000/Human_epidermal_growth_factor_receptor_2_positive.9.aspx.

[39] R Dhankhar *et al*. "Advances in novel drug delivery strategies for breast cancer therapy". In: Artificial Cells, Blood Substitutes, and Biotechnology (Oct. 2010). URL: https://www.tandfonline.com/doi/full/10.3109/10731199.2010.494578.

[40] R Felsted *et al*. "Protein N -Myristoylation as a Chemotherapeutic Target for Cancer". In: J Natl Cancer Institute (Nov. 1995).

[41] R Morimoto-Kamata *et al*. "Insulin-like growth factor-1 signaling is responsible for cathepsin G-induced aggregation of breast cancer MCF-7 cells". In: Cancer Science (May 2017). URL: https://doi.org/10.1111/cas.13286.

[42] R Rajala *et al*. "N-Myristoyltransferase". In: Molecular and Cellular Biochemistry (Jan. 2000). URL: https://link.springer.com/article/10.1023/A:1007012622030.

[43] R Rockne *et al*. " Introduction to Mathematical Oncology ". In: JCO Clinical Cancer Informatics (Apr. 2019). URL: https://ascopubs.org/doi/full/10.1200/CCI.19.00010.

[44] S Ali *et al*. "Estrogen Receptor Alpha in Human Breast Cancer: Occurrence and Significance". In: Journal of Memory Gland Biology and Neoplasia

(July 2000). URL: https://link.springer.com/article/10.1023/A:1009594727358.

[45] S Farabaugh *et al*. "Role of IGF1R in Breast Cancer subtypes, stemness and Lineage Differentiation". In: Front Endocrinol (2015). URL: https://pubmed.ncbi.nlm.nih.gov/25964777/.

[46] S Maurer *et al*. "N-terminal N-myristoylation of proteins: prediction of substrate proteins from amino acid sequence". In: Journal of Molecular Biology (Feb. 2019). URL: https://pubmed.ncbi.nlm.nih.gov/11955008/.

[47] S Maurer *et al*. "N-terminal N-myristoylation of proteins: refinement of the sequence motif and its taxon-specific differences". In: Journal of Molecular Biology (Apr. 2002). URL: https://pubmed.ncbi.nlm.nih.gov/11955007/.

[48] S Podell *et al*. "Predicting N-termial myristoylation sites in plant proteins". In: BMC Genomics (June 2004). URL: https://bmcgenomics.biomedcentral.com/articles/10.1186/1471-2164-5-37.

[49] S Weston *et al*. "Crystal structure of the anti-fungal target N-myristoyltransferase". In: Nature Structural and Molecular Biology (Jan. 1998). URL: https://www.nature.com/articles/nsb0398-213.

[50] U Das *et al*. "NMT in Encyclopedia of Signalling Molecules". In: NY Springer New York (2016). URL: https://doi.org/10.1007/978-1-4419-0461-4_100930.

[51] X Cui *et al*. "Biology of Progesterone Receptor Loss in Breast Cancer and its Implications for Endocrine Therapy". In: Journal of Clinical Oncology (Oct. 2005). URL: https://ascopubs.org/doi/full/10.1200/JCO.2005.09.004.

[52] Davide A Santeufemia Franco Lumachi. "Current Medical treatment of ER+ breast cancer". In: World Journal of Biological Chemistry (Aug. 2015). URL: https://www.wjgnet.com/1949-8454/full/v6/i3/231.htm.

[53] D. Hanahan and R. A. Weinberg. "Hallmark of Cancer: The Next Generation". In: Cell (Mar. 2011), pp. 646–674. URL: https://www.ncbi.nlm.nih.gov/pubmed/21376230.

[54] National Breast Cancer Foundation INC. "Breast Cancer Facts in the United States". In: (2020). URL: https://www.nationalbreastcancer.org/breast-cancer-facts.

[55] National Cancer Institute. "A to Z list of Cancer Types". In: National Cancer Institute (Jan. 1980). URL: http://www.cancer.gov/types.

[56] Dept. of Mathematics. "Modelling of neurons and carcinogenesis". In: University of Glasgow (Sept. 2008). URL: http://www.maths.gla.ac.uk/research/groups/biology/kal.htm.

[57] TN Tsangaris ML Palmer. "Breast biopsy in women 30 years old or less". In: The American Journal of Surgery (June 1993). URL: https://www.americanjournalofsurgery.com/article/S0002-9610(05)80793-7/pdf.

[58] Fatema Alamrawy Mohamed Nounou. "Breast Cancer: Conventional Diagnosis and Treatment Modalities and Recent Patents and Technologies". In: Breast Cancer: Basic and Clinical Research (Sept. 2015). URL: https://journals.sagepub.com/doi/10.4137/BCBCR.S29420.

[59] World Cancer Research. "Breast Cancer Statistics". In: World Cancer Research Fund (Aug. 2018), pp. 1236–1239. URL: https://www.wcrf.org/dietandcancer/cancer-trends/breast-cancer-statistics.

[60] Canadian Cancer Society. " Canadian Cancer Statistics 2019 ". In: Canadian Cancer Society's Advisory Committee on Cancer Statistics (Sept. 2019). URL: https://www.cancer.ca/~/media/cancer.ca/CW/cancer.

[61] Canadian Cancer Society. "Breast Cancer Stats in the Canada". In: (2020). URL: https://www.cancer.ca/en/cancer-information/cancer-type/breast/statistics.